GAS-PHASE ION CHEMISTRY OF HYDROXY AND AMINO-SUBSTITUTED INTERSTELLAR POLYCYCLIC AROMATIC HYDROCARBONS AND PROTONATED POLYCYCLIC AROMATIC HYDROCARBONS

Mélanie Ouellette

Thesis submitted to the
Faculty of Graduate & Postdoctoral Studies

In partial fulfillment of the requirements for
the degree of Master of Science

In the Ottawa-Carleton Chemistry Institute
Department of Chemistry, University of Ottawa
Ottawa, Ontario, Canada

June 2014

Candidate	Supervisor
Mélanie Ouellette	Dr. Paul M. Mayer

A mon père, Denis Ouellette et à ma mère, Andrée Ouellette

Abstract

The gas-phase ion chemistry of hydroxyl- and amino-substituted polycyclic aromatic hydrocarbons (PAHs) and their protonated counterparts were studied using mass spectrometry. Ions were generated using an electron ionization (EI) source and the unimolecular chemistry of metastable ions was studied by performing mass-analysed ion kinetic energy spectrometry (MIKES) experiments with a magnetic sector tandem mass spectrometer. Collision-induced dissociation (CID) experiments were used in conjunction with MIKES experiments to determine ion structure. The ten molecules studied were: 1-naphthol, 2-naphthol, 1-naphthylamine, 2-naphthylamine, 1-aminoanthracene, 2-aminoanthracene, 1-phenanthrol, 9-phenanthrol, 1-hydroxypyrene and 1-aminopyrene. Since it is believed that larger PAHs, on the order of more than 50 carbon atoms, populate the interstellar medium, the goal of this study was to attempt to extrapolate the results from smaller systems to larger ones. The trends found include: hydroxy-substituted PAH radical cations lose carbon monoxide spontaneously and amino-substituted PAH radical cations lose HCN. Mechanisms for both processes are proposed, and it appears from the present results that this process should extrapolate to larger PAHs. Another trend found was that all the remaining fragment ions were always a closed ring.

Protonated amino-substituted PAHs were generated by electrospray ionization using a quadruple time-of-flight mass spectrometer. By protonating 1-naphthol and 2-naphthol using methane in the high-pressure EI source, it was found that they lost exclusively H_2O. As for 2-naphthylamine, 1-aminoanthracene and 2-aminoanthracene, it was found that 2-naphthylamine lost NH_3 and a hydrogen atom, NH_3 being the dominant channel. However, as the ion size

increases, the hydrogen-loss channel became the dominant channel. This means that larger PAHs will likely lose exclusively a hydrogen atom to reform the parent radical cation.

Acknowledgements

I would like to thank Dr. Paul M. Mayer for giving me the opportunity to work on this project. He always had helpful tips, ideas and was always opened for new ideas. Also, I would like to thank Dr. Sander Mommers who assisted me with everything concerning the ZAB. He is very knowledgeable about everything in the laboratory and was a very helpful person to have around. I would also like to thank Brandi West who helped me numerous times when I started this project since she had experience with the instrument and the research. She provided her much appreciated time and guidance at the beginning of my learning. A special thank goes to my friends Jeffery Butson and Jenna Hamilton who provided their time for me when I needed it throughout this project. Jenna Hamilton is a good friend who was there for me when I needed it the most and who always believed in my abilities as a graduate student. Jeffery Butson is a friend who was always there to help me in my research ideas and would always be there when I needed it the most. I would like to thank Justin Renaud who provided guidance with the Q-TOF, with the breakdown diagrams and who was also there for me when I needed it. A special thank goes to Dr. John Holmes who proposed some experiments to help me confirm some questions I had throughout this project. I would also like to thank the Mayer lab who was a great help for ideas, support and who were great people to work with. I also want to thank my family and Pierre-Olivier Roy for believing in my capacities as a graduate student. A special thank goes to my best friend Karine Lacasse-Giroux who was always there for me and who believed in me throughout this project.

Table of Contents

A mon père, Denis Ouellette et à ma mère, Andrée Ouellette 1
Abstract 2
Acknowledgements 4
List of Figures 7
List of Tables 12
List of Abbreviations 13
Chapter 1. Introduction 15
1.1 Objectives 15
1.2 Interstellar Chemistry 16
1.3 Mass Spectrometry 18
1.3.1 Magnetic Sector Instrument – VG ZAB 19
1.3.2 Quadrupole time-of-flight mass spectrometer 28
1.3.2b Quadrupole mass filters 30
1.3.2d CID experiment and the breakdown diagram 32
Chapter 2. Experimental setup 33
2.1 VG-ZAB experiments 33
2.1 QTOF2 experiments 35
2.3 Calculations 38
Chapter 3. Radical Cations 40
3.1 –OH substituted PAHs 42
3.1.1 MIKES spectra 42
3.1.2 MI/CID spectra 46
3.1.3 CID spectra 50
3.1.4 Calculation results 51
3.1.5 Mechanisms 52
3.1.6 Extrapolation to larger PAHs 57

3.2 –NH2 substituted PAHs 58

3.2.1 MIKES spectra 58
3.2.2 MI/CID spectra 62
3.2.3 CID spectra 64
3.2.4 Calculation results 65
3.2.5 Mechanisms 66
3.2.6 Extrapolation to larger PAHs 69

Chapter 4. Protonated PAHs 70
4.1 Calculations 70

4.2 Protonation of 1-naphthol and 2-naphthol using the VG-ZAB 73

4.3 Protonation of the amines 77

Chapter 5. Conclusions 84
References 87

List of Figures

FIGURE 1: HISTOGRAMS OF THE PEAK WAVELENGTH OF THE UIR 6.2 M BAND (ON THE LEFT) AND 7.7 M (ON THE RIGHT). EACH FIGURE CORRESPONDS TO AREAS I, II, III, AND IV FROM TOP TO BOTTOM. THE DATA NUMBER IS NORMALIZED BY THE TOTAL NUMBER OF THE DATA WITHIN EACH AREA. 17

FIGURE 2: REVERSE GEOMETRY BE MAGNETIC SECTOR MASS SPECTROMETER SCHEME. NUMBER 1 REPRESENTS THE ION SOURCE, NUMBER 2 THE FOCUSING LENS, NUMBER 3 THE MAGNETIC SECTOR, NUMBER 4 THE 2ND FIELD-FREE REGION, NUMBER 5 THE BEAM RESOLVING SLITS, NUMBER 6 THE ELECTROSTATIC SECTOR AND NUMBER 7 THE MULTIPLIER DETECTOR. IN THE SECOND FIELD-FREE REGION, THERE ARE THE COLLISION CELLS AT NUMBER 8 AND THE BEAM DEFLECTION ELECTRODES AT NUMBER 9. 19

FIGURE 3: ELECTRON IONIZATION ION SOURCE SCHEME. NUMBER 1 REPRESENTS THE SOURCE BLOCK, NUMBER 2 THE FILAMENT, NUMBER 3 THE TRAP ELECTRODE, NUMBER 4 THE REPELLER ELECTRODE, NUMBER 5 THE ACCELERATION REGION AND NUMBER 6 THE FOCUSING LENS..... 20

FIGURE 4: DIFFERENT FRAGMENT ION PEAK SHAPES POSSIBLE IN A MIKES SPECTRUM. A) REPRESENTS A TYPICAL GAUSSIAN ENERGY PROFILE, B) KINETIC ENERGY RELEASE CAUSING DISCRIMINATION IN THE Z-AXIAL PLANE FOR FRAGMENT IONS (DISH-SHAPED PEAK), C) REPRESENTS COMPETING FRAGMENTATION CHANNELS RESULTING IN A COMPOSITE PEAK AND D) REPRESENTS FRAGMENTATION THAT OCCURED FROM A DISSOCIATIVE EXCITED STATE..... 26

FIGURE 5: SCHEMATIC OF THE Q-TOF2 MASS SPECTROMETER 28

FIGURE 6: QUADRUPOLE MASS FILTER WITH RODS SEPARATED BY A RADIUS R..... 31

FIGURE 7: QTOF 2 SETUP TO ATTEMPT PROTONATION USING ACID SPRAY 36

FIGURE 8: QTOF2 SETUP TO ATTEMPT PROTONATING USING ACID SPRAY. HERE IS SHOWN AN ATTEMPTED SETUP TO BUILD UP ACIDITY IN GAS FORM. 37
FIGURE 9: POSITIONAL ISOMERS EMPLOYED IN THIS THESIS 40
FIGURE 10: MIKES MASS SPECTRA OF THE 1-NAPHTHOL ION M/Z 144 (SHOWN CUT OFF TO EMPHASIS THE PRODUCT IONS). THE MASS SPECTRUM IN BLUE IS AT 8 KEV 42
FIGURE 11: MIKES SPECTRA OF 2-NAPHTHOL AFTER SELECTING THE PARENT ION (144 M/Z). THE SPECTRUM IN BLUE IS AT 8 KEV. (X) REFERS TO COLLISIONAL ARTIFACTS. 43
FIGURE 12: MIKES SPECTRA OF 1-PHENANTHROL AFTER SELECTING THE PARENT ION (194 M/Z). THE SPECTRUM IN BLUE IS AT 8 KEV 44
FIGURE 13: MIKES SPECTRA OF 9-PHENANTHROL AFTER SELECTING THE PARENT ION (194 M/Z). THE SPECTRUM IN BLUE IS AT 8 KEV 44
FIGURE 14: MIKES SPECTRA OF 1-HYDROXYPYRENE AFTER SELECTING THE PARENT ION (218 M/Z). THE SPECTRUM IN BLUE IS AT 8 KEV 45
FIGURE 15: MI/CID SPECTRA OF 1-NAPHTHOL, IN RED, AND 2-NAPHTHOL, IN BLUE, AFTER SELECTING THE FRAGMENT ION AT 116 M/Z 46
FIGURE 16: CID SPECTRA OF 1-PHENYL-1-PROPYNE, IN BLUE, AND INDENE, IN RED, AFTER SELECTING THE PARENT ION FOR EACH AT 116 M/Z 47
FIGURE 17: MI/CID SPECTRUM FOR 1-PHENANTHROL AFTER SELECTING THE FRAGMENT ION AT 166 M/Z 48
FIGURE 18: CID SPECTRUM OF FLUORENE IN BLUE AND CID SPECTRUM OF 9-PHENANTHROL WHEN SELECTING DIRECTLY 166 M/Z FROM THE SOURCE IN PINK 49
FIGURE 19: MI/CID SPECTRUM OF 1-HYDROXYPYRENE AFTER SELECTING THE FRAGMENT ION AT 190 M/Z 50

Figure 20: Structure of indene (left) and 1-phenyl-1-propyne (right). 51
Figure 21: Proposed mechanism for the loss of CO for 1-naphthol 53
Figure 22: Proposed mechanism for the loss of CO for 2-naphthol 54
Figure 23: Proposed mechanism for the loss of CO for 1-phenanthrol 55
Figure 24: Proposed mechanism for the loss of CO for 9-phenanthrol 56
Figure 25: Proposed mechanism for the loss of CO for 1-hydroxypyrene 57
Figure 26: MIKES spectra of 1-naphthylamine after selecting the parent ion (143 m/z). The spectrum in blue is at 8 keV. Some H loss was also observed. 59
Figure 27: MIKES spectra of 2-naphthylamine after selecting the parent ion (143 m/z). The spectrum in blue is at 8 keV. Some H loss is also observed. 60
Figure 28: MIKES spectra of 1-aminoanthracene after selecting the parent ion (193 m/z). The spectrum in blue is at 8 keV..... 61
Figure 29: MIKES spectra of 2-aminoanthracene after selecting the parent ion (193 m/z). The spectrum in blue is at 8 keV..... 62
Figure 30: MI/CID spectra of 1-naphthylamine, in blue, and 2-naphthylamine, in red, after selecting the fragment ion at 116 m/z 63
Figure 31: MI/CID spectra of 2-aminoanthracene, in red, and 1-aminoanthracene, in blue, after selecting the fragment ion at 166 m/z 64
Figure 32: Proposed mechanism for the loss of HCN for 1-naphthylamine 66
Figure 33: Proposed mechanism for the loss of HCN for 2-naphthylamine 67
Figure 34: Proposed mechanism for the loss of HCN for 1-aminoanthracene 67
Figure 35: Proposed mechanism for the loss of HCN for 2-aminoanthracene 68
Figure 36: Proposed mechanism for the loss of HCN for 1-aminopyrene 68

FIGURE 37: MIKES SPECTRUM DEPICTING THE RELATIVE INTENSITY OF THE M+1 PEAK BEING A MIX OF $[M+H]^+$ AND $^{13}C\ M^{+\cdot}$ AND THE $M^{+\cdot}$ PEAK 73

FIGURE 38: MIKES SPECTRUM OF PROTONATED 2-NAPHTHOL AFTER SELECTING M/Z 145. (X) SHOWS COLLISIONAL ARTIFACTS 74

FIGURE 39: GRAPH SHOWING THE PROTONATION OF 1-NAPHTHOL USING METHANE AS A CHEMICAL IONIZATION GAS. THE RATIOS BETWEEN LOSS OF 18 M/Z AND 28 M/Z WERE PLOTTED AS A FUNCTION OF THE RATIO OF THE M+1 PROTONATED PEAK TO THE PARENT ION PEAK M..... 75

FIGURE 40: GRAPH SHOWING THE PROTONATION OF 2-NAPHTHOL USING METHANE AS A CHEMICAL IONIZATION GAS. THE RATIOS BETWEEN LOSS OF 18 M/Z AND 28 M/Z WERE PLOTTED AS A FUNCTION OF THE RATIO OF THE M+1 PROTONATED PEAK TO THE PARENT ION PEAK M..... 76

FIGURE 41: PROPOSED MECHANISM FOR THE LOSS OF WATER FROM PROTONATED 1-NAPHTHOL ... 77

FIGURE 42: PROPOSED MECHANISM FOR THE LOSS OF WATER FROM PROTONATED 2-NAPHTHOL ... 77

FIGURE 43: PROPOSED MECHANISM FOR THE LOSS OF AMMONIA FROM PROTONATED 2-NAPHTHYLAMINE 78

FIGURE 44: PROPOSED MECHANISM FOR THE LOSS OF HYDROGEN FROM PROTONATED 2-NAPHTHYLAMINE. THE FIRST POSSIBILITY IS PROTON LOSS FROM THE NH_3 GROUP (TOP) AND THE SECOND POSSIBILITY IS HYDROGEN LOSS FOR THE AROMATIC RING (BOTTOM). 79

FIGURE 45: BREAKDOWN DIAGRAM OF PROTONATED 2-NAPHTHYLAMINE USING MS/MS ON A Q-TOF INSTRUMENT. THE COLLISION ENERGY USED WAS FROM 6.00 TO 35.00 EV (E LAB.) BY INCREMENTS OF 1. THE BREAKDOWN DIAGRAM WAS PLOTTED USING THE RELATIVE INTENSITIES OF EACH FRAGMENT ION. 80

FIGURE 46: BREAKDOWN DIAGRAM OF PROTONATED 2-AMINOANTHRACENE USING MS/MS ON A Q-TOF INSTRUMENT. THE COLLISION ENERGY USED WAS FROM 6.00 TO 35.00 EV (E LAB.) BY

increments of 1. The breakdown diagram was plotted using the relative intensities of each fragment ion. 81

Figure 47: Proposed mechanism for the loss of ammonia from protonated 2-aminoanthracene 82

Figure 48: Proposed mechanism for the loss of a hydrogen from protonated 2-aminoanthracene. The first possibility is hydrogen loss from the NH_3 group (top) and the second possibility is hydrogen loss for the aromatic ring (bottom). 82

List of Tables

TABLE 1: PROTON AFFINITIES (EV) OF THE PAHS STUDIED IN THIS THESIS, CALCULATED USING TWO DIFFERENT METHODS 71

List of Abbreviations

CI	Chemical ionization
CID	Collision-induced dissociation
DFT	Density functional theory
EI	Electron impact
ESA	Electrostatic analyser
ESI	Electrospray ionization
FFR	Field-free region
FUV	Far-ultraviolet-pumped
IR	Infrared
ISM	Interstellar Medium
MI/CID	Mass-analysed ion/collision-induced dissociation
MIKES	Mass-analysed ion kinetic energy spectrometry
MP2	Second order Moller-Plesset perturbation theory
MS	Mass spectrometry
PAH	Polycyclic Aromatic Hydrocarbon
QTOF	Quadrupole time-of-flight mass spectrometer
THF	Tetrahydrofuran

TOF	Time-of-flight
ZAB	Zero aberration

Chapter 1. Introduction

1.1 Objectives

The goal of this thesis is to explore the gas-phase ion chemistry of small polycyclic aromatic hydrocarbon (PAH) ions. This class of molecules is believed to account for twenty percent of the organic carbon in the interstellar medium.[1 2] Since PAHs (neutral and ions) are suggested to play a significant role in the chemistry of the interstellar medium, the reactivity of such ions were explored.[3] These molecules are believed to behave as catalysts for the formation of small molecules like H_2, H_2O, NH_3, etc by acting as surrogate surfaces. In this case, hydroxylated and aminated PAHs could be intermediates in the larger catalytic mechanism. Thus, we are examining the fate of these intermediates by studying the unimolecular chemistry of hydroxy and amino substituted PAHs and their protonated counterparts. The PAHs studied were those available for purchase and cover a small range of PAH size from naphthalene to pyrene: 1-naphthol, 2-naphthol, 1-naphthylamine, 2-naphthylamine, 1-phenanthrol, 9-phenanthrol, 1-aminoanthracene, 2-aminoanthracene, 1-hydroxypyrene and 1-aminopyrene. The chemistry of these ions probes the first step in H_2O and NH_3 formation, that is the intermediate first formed by OH and NH_2 substitution on the PAH ring system. The next step would be the addition of hydrogen, and we selected to protonate the substituted PAHs to generate ionic species that could possibly lose H_2O and NH_3. Two mass spectrometers were employed: a modified VG ZAB magnetic sector instrument for the study of mass selected radical cations formed by electron ionization and protonated hydroxyl-PAHs by chemical ionization, and a Micromass Q-TOF 2 mass spectrometer equipment with an electrospray ionization source for the study of protonated amino-PAHs. The Gaussian 09 suite of programs was used to perform

calculations on all PAHs, their protonated counterparts and on their fragments to have a better understanding of the chemistry and energetics of the way they break down. Extrapolation of the results to larger PAHs can be possible if a trend is found in the small PAHs which in this study have a maximum of four aromatic rings.

1.2 Interstellar Chemistry

Ground-base and airborne studies in the 1970s using infrared (IR) spectroscopy have shown some broad emission features located in mid-infrared region of the IR (Figure 1).[4 5] These IR spectra were collected in the bright HII regions, planetary nebulae and reflection nebulae. All IR spectra were showing the same features and bands, thus the region of the interstellar medium (ISM) where they were measured did not matter. Arising from this observation, a great interest was developed in the assignment of the mid-infrared bands of these IR spectra. After further investigation, the broad features showing on the IR spectra were believed to be from the combined IR fluorescence of a multitude of far-ultraviolet-pumped (FUV) polycyclic aromatic hydrocarbons (PAH), mostly from those of at least 50 atoms of carbon like fullerene.[6] The argument for these assignments was made by stacking the IR spectra of many PAHs on top of another and concluding that the profile of the bands was present in the same manner as in the IR spectra collected from observations. From this reasoning, PAHs are believed to account for about twenty percent of the organic carbon in the interstellar medium. Thus, an open question is how PAHs would play a role in the gas-phase ion chemistry of the ISM. These molecules are present in the heating of neutral gas and in the ionization balance in molecular clouds, making them potentially extremely important in the ion-molecule chemistry of gas-phase species present in the ISM.

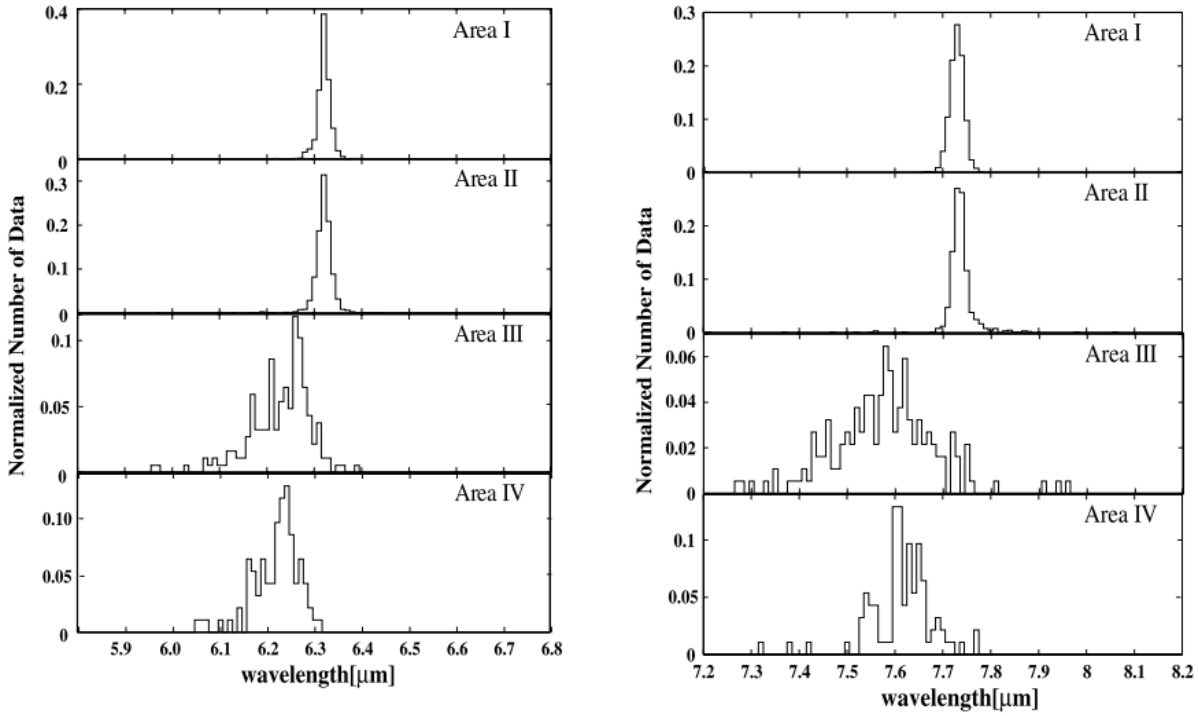

Figure 1: Histograms of the peak wavelength of the UIR 6.2 m band (on the left) and 7.7 m (on the right). Each figure corresponds to areas I, II, III, and IV from top to bottom. The data number is normalized by the total number of the data within each area.[7]

PAHs possess key features that make them viable in the ISM. They are from the hydrocarbon family and thus are mostly composed of carbons and hydrogens. These carbons and hydrogens are arranged in fused benzene rings with peripheral hydrogens. The π system formed by the network of fused benzene rings form rigid and stable species. They also show a very planar nature and can thus be stacked in clusters bonded by Van Der Waals interactions. Some PAHs have one hydrogen substituted for a methyl group or hydroxy group or in some cases, one carbon can possess two hydrogens, which is called a superhydrogenated PAH. Given the very low vapor pressure of PAHs over 50 carbons, which makes them difficult to make in the

gas phase, studies have been conducted using smaller PAHs. Studies performed on positively ionized PAHs were conducted since ionic species are believed to participate in the IR spectra.

1.3 Mass Spectrometry

The technique used in this thesis to study PAHs is mass spectrometry. As stated above, this technique is used for its properties similar to the interstellar environment: low pressure. This technique also permits ionization in the gas phase, an essential property that the technique must possess for this type of study. Mass spectrometry is an analytical technique used to get information about the mass-to-charge ratio of ionized molecules. The sample used can be solid, liquid or gas as long as it can be ionized in the gas phase. The way the results are produced is by producing a mass spectrum of the intensity vs the mass-to-charge when certain ions hit the detector. Mass spectrometry is not an optical technique in the sense that there is no photon involved. Depending on the system studied, the chemist will need to use a specific mass spectrometer. For this study, replicating the conditions of the interstellar medium is essential to ensure proper comparison with data collected previously. The instrument mostly used in this study is a modified VG ZAB magnetic sector instrument. What differentiates the ZAB sector instrument from other mass spectrometers is that it allows for the study of the spontaneous dissociation of metastable ions. Spontaneous dissociation is a must given that molecules and ions are very far from one another in the interstellar medium and their likelihood of hitting one another is very low.

1.3.1 Magnetic Sector Instrument – VG ZAB

The sector instrument used in this study is a VG-ZAB sector instrument. It is a mass spectrometer consisting of both a magnetic and electrostatic sector. It is thus a double-focusing mass spectrometer since the ion beam can be focused at two places in the apparatus. The VG-ZAB used is a reverse-geometry tandem sector mass spectrometer of BE configuration. Here is a scheme of a reverse-geometry mass spectrometer.[8]

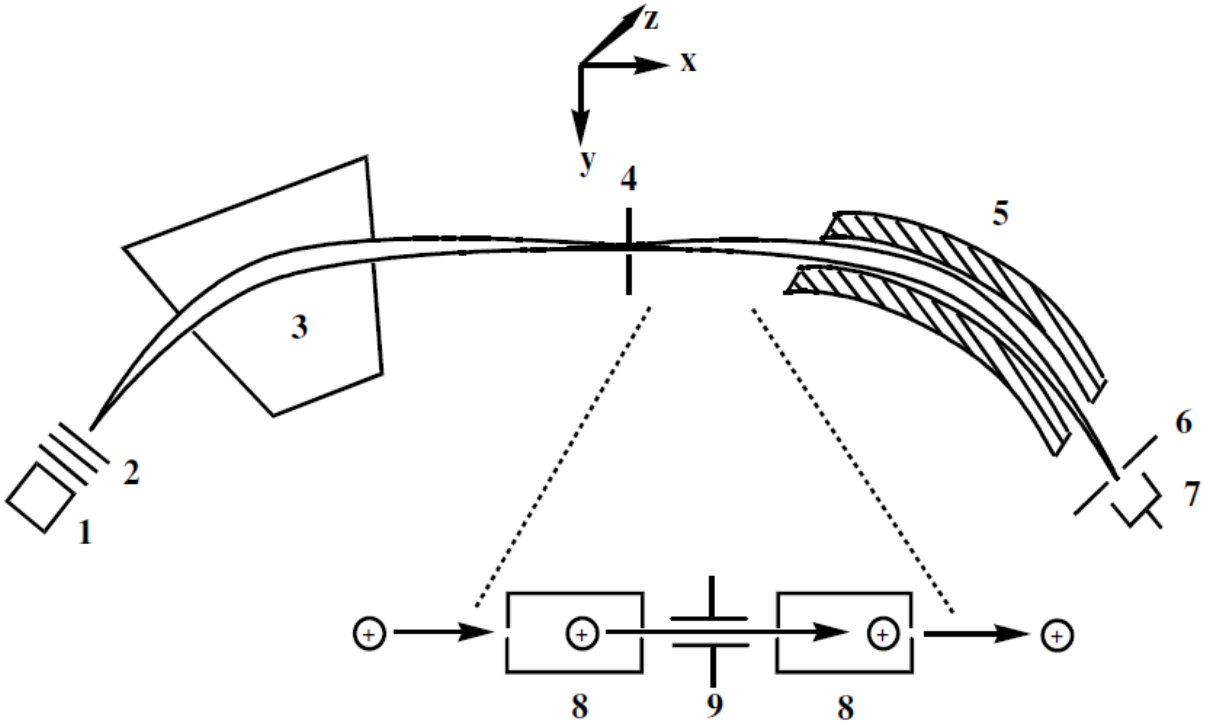

Figure 2: Reverse geometry BE magnetic sector mass spectrometer scheme. Number 1 represents the ion source, number 2 the focusing lens, number 3 the magnetic sector, number 4 the 2nd field-free region, number 5 the beam resolving slits, number 6 the electrostatic sector and number 7 the multiplier detector. In the second field-free region, there are the collision cells at number 8 and the beam deflection electrodes at number 9.[8]

1.3.1a Ion Sources

To be able to perform an experiment, an ion source is needed. The three ion sources used were an electron ionization (EI) source, a chemical ionization (CI) source and a high-pressure source.

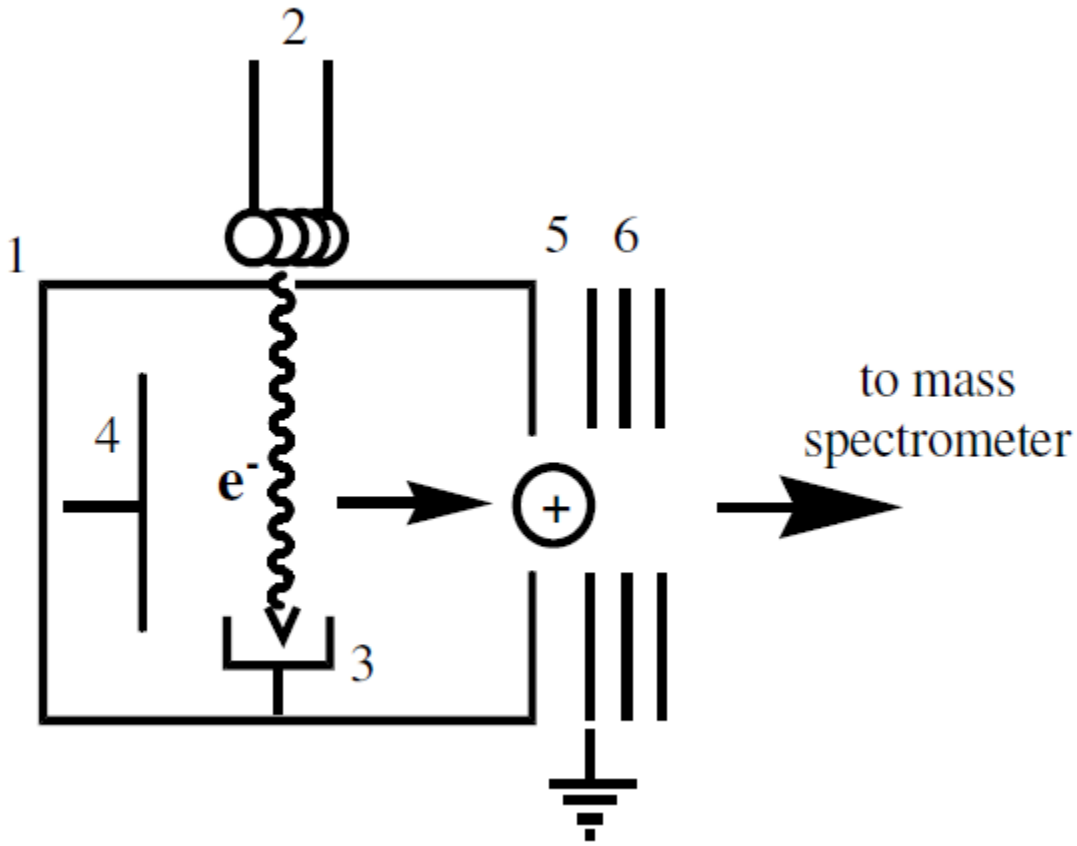

Figure 3: Electron ionization ion source scheme. Number 1 represents the source block, number 2 the filament, number 3 the trap electrode, number 4 the repeller electrode, number 5 the acceleration region and number 6 the focusing lens.[8]

Using an EI source, the sample can be introduced as a liquid or a solid in the source with the help of an inlet. All PAHs studied were a solid. The vapor pressure of the solid is important

since it determined the amount of sample introduced in the ion source. The molecules in the gas phase in the source are ionized by electrons accelerated in the direction of the block using a potential gradient. The electrons are produced by heating the filament in the source and are collected in the trap electrode. The ions exit the source by the help of a repeller electrode through the exit slit. The VG-ZAB used in this study can have ions accelerated between 6 keV and 9 keV by increments of 1 keV. The real acceleration energy is a bit less since the repeller is used to push the ions forward and ions naturally lose a bit of energy by colliding, breaking apart, ionizing, etc. A pressure of around 6-7 mTorr is expected in the EI source. The electron energies used in this instrument are around 70 eV. This results in a broad energy distribution that is a non-Boltzmann distribution, making the discussion of the ion chemistry related to thermodynamic temperature rather difficult.

In the CI source, a gas is introduced. In this study, the gas is methane. The methane will get ionized by electron ionization and charge transfer to our molecule (M) after a series of steps. Here is the general CI route using methane.

$$CH_4 + e^- \rightarrow CH_4^+ + 2e^-$$

$$CH_4 + CH_4^+ \rightarrow CH_5^+ + CH_3$$

$$M + CH_5^+ \rightarrow CH_4 + MH^+$$

The last source used was the high pressure source. This source was used to protonate the molecules used in this study. The reason of using this source is that the pressure is greatly

augmented within it, helping the protonation. The high pressure source used has only three small orifices and the slit used is very small to help build up the pressure in the source. The second orifice is to permit the vapor pressure from our sample to enter the source and the third orifice is to enable the gas used to protonate, methane, to enter the source. The pressure can be raised to about 4-5 Torr to get adequate protonation depending on the sample used. Usually, the settings are really different from the simple EI source to get the ions to penetrate and ionize the sample and effectively leave the source.

1.3.1b The Magnetic Sector

The second part of the VG-ZAB reverse-geometry mass spectrometer is the magnetic sector. Two parallel electromagnets surround an iron core in the magnetic sector. The magnetic field generated by magnet is perpendicular to the flight direction of the ion beam. This path is said to be orthogonal to the magnetic field and is described by this relationship[8]:

$$r = \frac{m\upsilon}{Bze}$$

The radius of the curvature of the ion path is *r*, the ion mass is *m*, the velocity is v, the magnetic field strength is *B*, the number of charges of the ion is *z* and the elementary charge is *e*. The VG-ZAB used has a fixed radius of curvature *r*. How it works is by passing ions of a particular momentum *m*v by selecting a specific magnetic field strength *B*. Thus, the magnetic is

used to select ions by their momentum and not their mass. Since the ion sources used operate between 6 keV and 9 keV for the magnetic sector used, the ion kinetic energy must be taken into account. The velocity becomes:

$$\upsilon = \sqrt{\left(\frac{2zeV}{m}\right)}$$

resulting in the final equation by rearranging equation (#):

$$m/z = \frac{B^2 r^2 e}{2V}$$

1.3.1c The Field-Free Region

The third part of the VG-ZAB mass spectrometer is the field-free region (FFR). The instrument used is composed of three FFRs[8]. They are located between the ion source and magnetic sector, between the magnetic sector and first electrostatic sector, and between the first electrostatic sector and second electrostatic sector. In the FFR, there are collision cells and ion beam deflection electrodes to adjust the ion beam path. The collision cells are used to perform certain experiments which will be discussed later. Those collision cells are made of steel about two or three centimeters with a hole for the ion beam to pass through. A collision gas can be introduced in the collision cell to perform several types of experiments like collision-induced dissociation (CID) and mass-analysed ion kinetic energy spectrometry followed by collision-induced dissociation (MI/CID). These experiments will be discussed later.

1.3.1d The Electrostatic Sector

The fourth part of the VG-ZAB is the electrostatic sector (ESA)[8]. In the ESA, a potential difference is applied between two curved parallel plates. This produces an electric field with a strength *E*. The ion beam that passed through the ESA follows the following relationship:

$$\frac{1}{2}\, m\upsilon^2 \;=\; zeV \;=\; \frac{1}{2}\, zeEr$$

Ions of selected translational kinetic energy are able to pass through. They are then focused and hit the detector that monitor the flux of ions. The software then converts the translational energy into mass-to-charge to produce the spectrum collected.

1.3.1e Mass-analysed ion kinetic energy spectrometry (MIKES)[8]

It takes the ions several microseconds to arrive in the FFR of the VG-ZAB while accelerated out of the ion source with keV translational kinetic energies. Given this timescale, the ions dissociating during this timeframe are called metastable ions. A^+ and B, which are the unimolecular decomposition fragments of the metastable ion AB^+ will show lower translational kinetic energy T because of the conservation of energy and momentum. These equations illustrate this:

$zT_A{}^+ = 1/2\ m_{A+} \cdot\ \upsilon^2$ $\qquad$ $zT_B = 1/2\ m_B \cdot \upsilon^2$ $\qquad$ $zT_{AB}{}^{+\cdot} = 1/2\ m_{AB}\ \upsilon^2$

where z is the number of charges, T is the translational kinetic energy, m refers to the mass of the species in question and υ is their velocities.

Thus, we obtain:

$$T_A^+ = \frac{m_A^+}{m_{AB}^{+\cdot}} T_{AB}^{+\cdot}$$

The fragments ions, since they possess lower translational energies, will pass in sequence through to the detector when scanning the ESA. Also, since this experiment occurs on the microseconds timescale, if isomeric ions interconvert during that timescale, they will have almost identical MIKES spectra. During a MIKES experiment, there are several characteristic peak shapes that are expected. As shown in figure 4 below there is a typical Gaussian energy profile peak. This peak changes if there is a large average kinetic energy release that causes the fragment ions to have z-axial discrimination, making the peak dished-shaped. Moreover, another possible shape is possible when two competing channels are superimposed. This produces a composite peak. Finally, another peak is possible when the fragment ions were the result of a dissociative excited state and does not resemble a Gaussian profile.

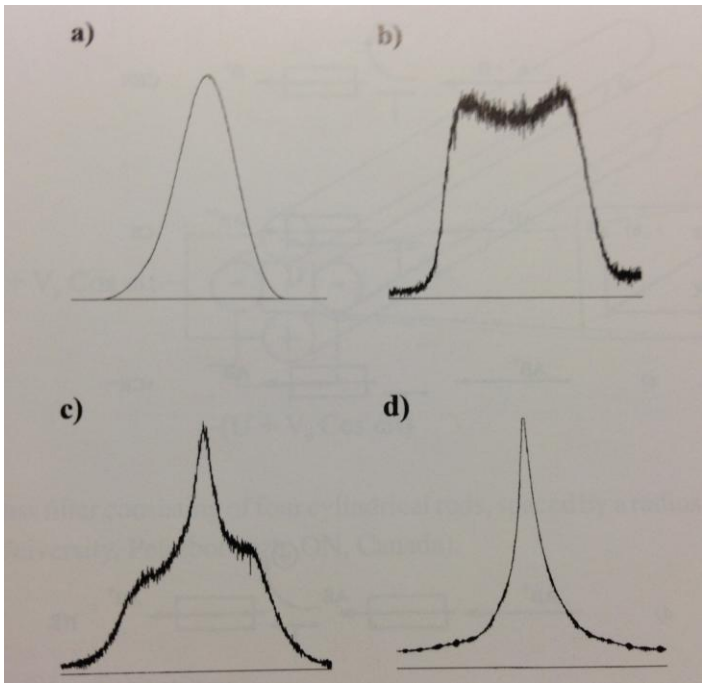

Figure 4: Different fragment ion peak shapes possible in a MIKES spectrum. a) represents a typical Gaussian energy profile, b) kinetic energy release causing discrimination in the z-axial plane for fragment ions (dish-shaped peak), c) represents competing fragmentation channels resulting in a composite peak and d) represents fragmentation that occured from a dissociative excited state.[8]

1.3.1f Collision-induced dissociation mass spectrometry (CID)[8]

By introducing a target gas into a collision cell in one of the FFR and by mass selecting ions before colliding them with that target gas, a collision-induced mass spectrum is obtained. This is achieved by producing a 10% beam reduction using the target gas desired, usually helium. The CID mass spectra are obtained and analysed the same way as MIKES spectra, but they represent a different situation. Those spectra represent all the possible dissociation processes of the precursor ion, which is very different from MIKES experiments. New and

important information can be obtained by performing CID on the precursor ion since the timescale is very different from MIKES experiments. They range from the time of the collision with the target gas to the time ions leave the FFR the collision cell was in. Since the timescale is shorter, and ion internal energy higher, isomerization does not have a chance to compete with bond cleavage, making keV CID mass spectra characteristic of ion connectivity.

1.3.1g Mass-analysed ion kinetic energy spectrometry followed by collision-induced dissociation

Another experiment that can be done on the VG-ZAB is to do a MIKES experiment followed by a collision-induced dissociation. This experiment is helpful when comparing fragments of different precursor ions that have the same m/z to see if those fragments have the same connectivity. The chosen fragment ion is formed by the dissociation of the precursor ion in a MIKES experiment and is then selected with the first ESA. Target gas is introduced in a collision cell in the 3rd FFR. The third ESA is scanned and the ions hit the detector. Since CID spectra are characteristic of ion connectivity, they can be compared to other fragment ions of the same m/z.

1.3.2 Quadrupole time-of-flight mass spectrometer

Protonated amino PAHs were studied on a Micromass quadrupole time-of-flight mass spectrometer (QTOF2) shown in figure 5. The components will be addressed below.

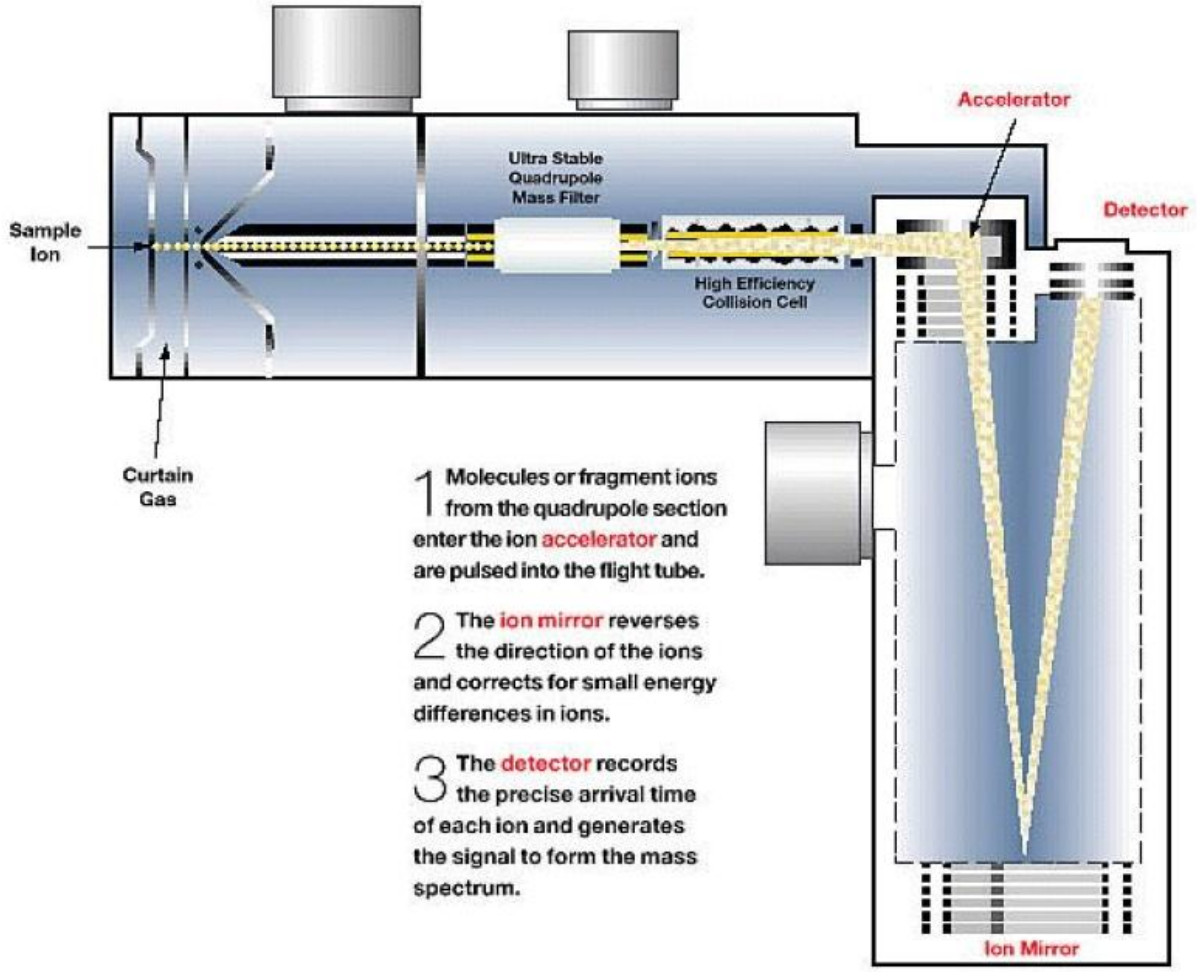

Figure 5: Schematic of the Q-TOF2 mass spectrometer[8]

1.3.2a Electrospray ionization (ESI)

Electrospray ionization (ESI) was developed by John Bennett Fenn in 1984. He received the Nobel Prize in Chemistry in 2002 for the development of the ESI source.

The way the ions are made is what distinguishes this source from an EI source used in a VG-ZAB sector instrument. The ions are produced in sequence. A solution of the analyte is made and an acid might be introduced to help the production of ions if the analyte is polar. The solution is then injected to a metal tube capillary using a flow from 1 µL/min to 1 mL/min.

An electric potential is applied to the tip of the capillary and a gas passes around the capillary, which is usually N_2. The source can be set to positive or negative mode. For example, in the positive mode, the tip will have a high electric potential applied to it making the positive ions travel further away from the tip and the negative ions stick to the tip. The liquid will expand since the accumulated positive charges will repel each other and a Taylor cone will be formed. The Taylor cone forms when the expanded liquid has the force of the accumulated positive charges equal to the surface tension of the liquid. The Taylor cone will break down into positively-charged droplets due to the high electric potential of the tip and those droplets will be sprayed. The solvent in the droplets will start to evaporate, making the droplets shrink. As they continue to shrink, the Coulomb repulsion becomes greater than the surface tension for each droplet since the surface charge to surface area increases. This makes the droplets dissociate into smaller droplets and is called Coulomb explosion. This phenomenon continues until gas-phase ions are produced without any solvent remaining.

1.3.2b Quadrupole mass filters

In a quadrupole mass filter, the potential ϕ in the field is represented by the following equation:

$$\phi = \frac{\phi_0}{r_0^2}(ax^2 + by^2 + cz^2)$$

ϕ_0 is the applied potential, the distance between the hyperbolic rods is shown by r_0 and the coefficients are represented by a, b and c. This applied potential is the radio-frequency potential (RF), V cos ωt and the direct current (DC) potential U combined. This relationship is expressed by the following equation:

$$\phi = U + V\cos\omega t$$

The angular frequency of the radio-frequency field is expressed by ω and is $2\boldsymbol{\pi}$ times the frequency in Hertz. A hyperbolic geometry is preferred for the rods in a quadrupole mass filter. The most common arrangement is four cylindrical rods which are separated by a distance of 2r where r = 1.16 r_0. With this geometry, an acceptable field geometry along the axis of the mass filter is created. The field along the axis of the instrument is non-existent, simplifying the equation to:

$$\phi = \frac{\phi_0}{r_0^2}(ax^2 + by^2)$$

1 is the value given to a and -1 is the value given to b in this case. The equation then becomes:

$$\phi = \frac{\phi_0}{r_0^2}(x^2 - y^2)$$

In this field, the equations of motion are as followed:

$$\frac{d^2x}{dt^2} + \frac{e}{mr_0^2}(U - V\cos\omega t)x = 0$$

Here is a schematic of a quadrupole mass filter:

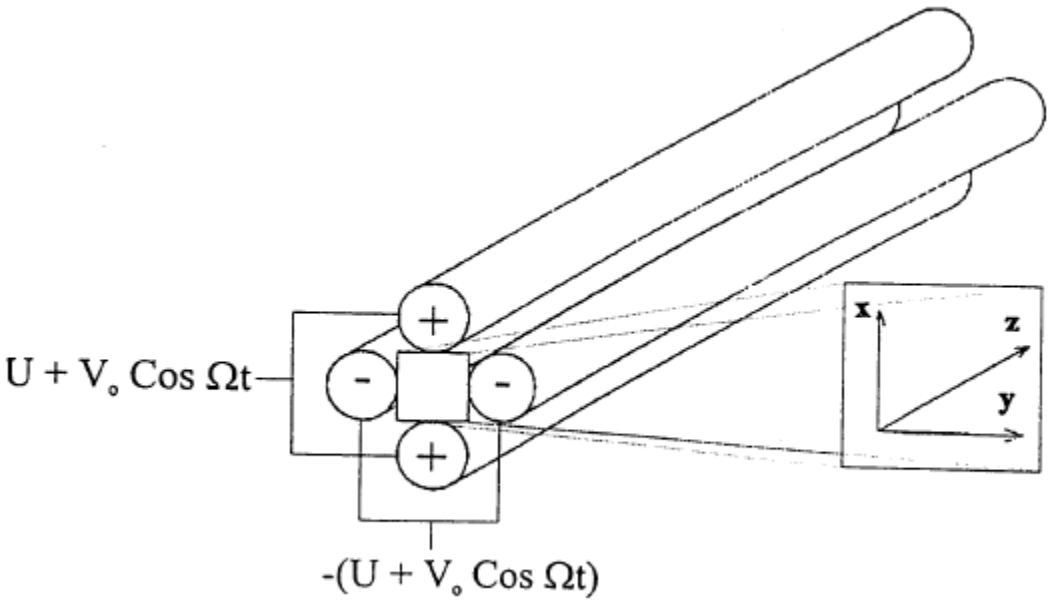

Figure 6: Quadrupole mass filter with rods separated by a radius r[8]

1.3.2c Time-of-flight mass spectrometry (TOF)

During a time-of-flight mass spectrometry experiment, large ions having the same kinetic energy as small ions will travel slower since they possess lower velocities. The equation used is the one for kinetic energy:

$$zeV = \frac{1}{2}m\upsilon^2$$

The time the ions take to travel is represented by the following equation:

$$td = d\frac{m}{2zeV}$$

The time the ions take from the ESI source to the detector is given by t_d, the potential drop is V and the translational kinetic energy of ions which are accelerated from the ESI source is given by zeV.

1.3.2d CID experiment and the breakdown diagram

This mass spectrometer is useful to create breakdown diagrams of the ions studied. To create such a breakdown diagram, a mass spectrum is collected at each lab frame collision energy in eV between an interval of center-of-mass collisional energies at a set increment. After collecting information on the relative intensities of each fragment and on the parent ion, a figure is created plotting the relative intensity on the center-of-mass collision energy.

Chapter 2. Experimental setup

2.1 VG-ZAB experiments

1-naphthol, 2-naphthol, 1-naphthylamine, 2-naphtylamine, 1-phenanthrol, 9-phenanthrol, 1-aminoanthracene, 2-aminoanthracene, 1-hydroxypyrene, 1-aminopyrene, indene, 1-phenyl-1-propyne and fluorene were purchased at Sigma-Aldrich.[910] They were used without further purification. For MIKES experiments, a source using 7 eV, 8 eV and 9 eV was used. The CID cell was not filled with any gas and the molecular ions were allowed to dissociate spontaneously in the 2nd FFR. For 1-naphthol and 2-naphthol, the mass which the magnet was set was 144 m/z for each of the voltages used. For 1-naphthylamine and 2-naphthylamine, the magnet was set to a mass of 143 m/z for each voltages used. For 1-phenanthrol and 9-phenanthrol, the magnet was set at 194 m/z. For 1-aminoanthracene and 2-aminoanthracene, the mass used for the magnet was 193 m/z for each of the voltage. For 1-hydroxypyrene, the mass used was 218 m/z for the magnet at each voltages, and finally for 1-aminopyrene, the mass used was 217 m/z for the magnet for each voltages. All these molecules are solids at room temperature and a solid probe was used to insert the samples into the instrument. The pressure of the source on the gage of the instrument while doing MIKES experiments was between 1.0×10^{-6} Torr and 9.0×10^{-6} Torr. Each MIKES experiment was repeated at 10 times and 100 times amplification to know the relationship between the parent ion and the fragments in terms of relative intensities. The first ESA was used to scan the kinetic energy and then, each fragment ion hit the detector with its respective parent ion.

Afterwards, CID experiments were performed on each of the previously mentioned molecular ions. The only difference in terms of experimental setup was that a gas was introduced in one of the collision cells in the 2nd FFR. This gas was helium. This experiment was used to determine the full fragmentation pattern of each molecular ion. This experiment was also performed on indene, 1-phenyl-1-propyne and fluorene, which are possible fragments during the MIKES experiments on 1-naphthol, 2-naphthol, 1-naphthylamine, 2-naphthylamine and 9-phenanthrol, to determine if these were the fragments seen in the MIKES spectra of each parent ion.

Afterwards, MI/CID experiments were performed on each molecular ion mentioned previously except indene, 1-phenyl-1-propyne and fluorene. The setup was the same as a MIKES experiment except that the fragment of interest is selected in the first ESA and allowed to go through the 3rd FFR. In the 3rd FFR, one of the cells is filled with helium and the 2nd ESA is used to scan. All fragments hit the detector. This experiment is used to compare the fragmentation pattern to the CID experiments of indene, 1-phenyl-1-propyne and fluorene to determine if the three molecular ions can be the fragment ions seen in the spectra during the MIKES experiments.

A last experiment was performed on the VG-ZAB. Protonation was performed on 1-naphthol and 2-naphthol using a high-pressure source and methane. Methane was introduced as a gas using the gas inlet provided and the high-pressure source was introduced in the instruments using the CI slit. The pressure of the source on the gage was between 1.0 x $10^{\wedge -5}$ Torr and 9.0 x

$10^{\wedge -4}$ Torr depending on the experiment done. The protonation was monitored using the ratio of the M+1 parent ion peak over the parent ion peak M. Protonation was possible between 15% and 100%. Then, the experiment was performed as a normal MIKES experiment and a spectrum was collected. The ratio between water loss and carbon monoxide loss was measured. This experiment is performed to study if the M+1 protonated peak only leads to loss of water or if the loss of carbon monoxide is also a fragment. Protonation on 1-naphtylamine and 2-naphthylamine was also performed but not successful. Protonation was also performed on the bigger molecules but not successful.

2.1 QTOF2 experiments

Protonation experiments were performed using the QTOF2. These were only successful for 1-naphthylamine, 2-naphthylamine, 1-aminoanthracene and 2-aminoanthracene. The solution used was at 0.1 mg/mL of each molecule of interest in a solution of 40:60 THF:Methanol. Using ESI, the protonated molecular ions were allowed to dissociate using CID. The collision gas used was argon. The breakdown diagram was done on each molecule using collision energies between 6 eV and 35 eV. To create these breakdown diagrams, a mass spectrum is collected at each increment of 1 eV between 6 and 35 eV. Relative intensities of each fragment and of the parent ion are calculated for each spectrum. Then, a figure is created plotting the relative intensity on the center-of-mass collisional energy. The processed is repeated for each molecular ion studied.

Protonation was attempted on 1-naphthol and 2-naphthol using an Acid Spray setup.

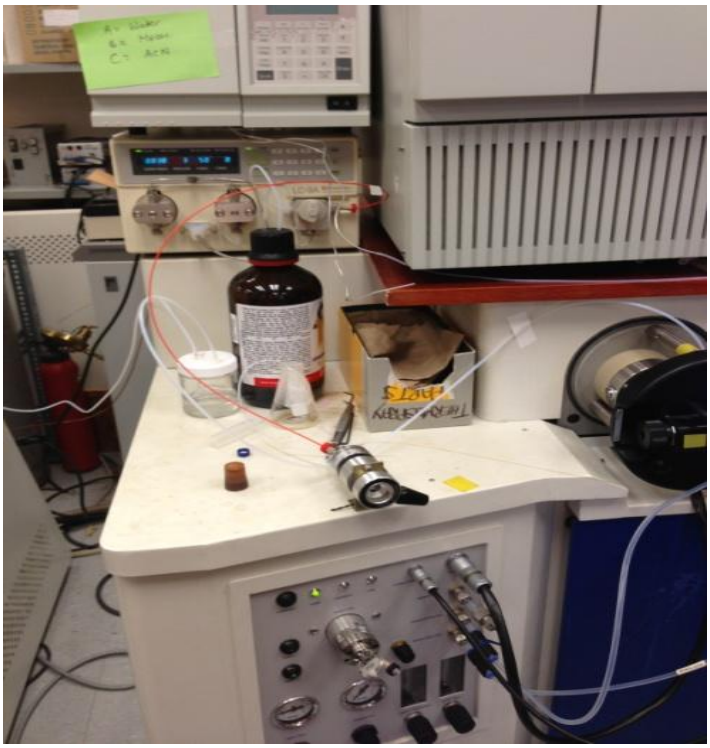

Figure 7: QTOF 2 setup to attempt protonation using acid spray

Figure 8: QTOF2 setup to attempt protonating using acid spray. Here is shown an attempted setup to build up acidity in gas form.

The solution was prepared at 0.1 mg/mL using 40:60 THF:Methanol. The ESI gas, nitrogen, was introduced in a container which had glacial acetic acid to help protonation. The resulting gas was then used to spray using the ESI source. Unfortunately, protonation was not possible on 1-naphthol and 2-naphthol.

2.3 Calculations

Two methods were used in this study. The first one was the MP2 method or Møller-Plesset perturbation theory. This method is a post Hartree-Fock ab initio method that add electron correlation to the original Hartree-Fock method. The electron correlation is added using Rayleigh-Schrödinger perturbation theory. Perturbation theory is used to find an approximate solution to a system that cannot be solved exactly. The system starts with a simple model and Hamiltonians are added until the system becomes a little more complex or perturbed. The MP2 method is of the second order.

The second method used was the DFT method or density functional theory using B3LYP or Becke, three-parameter, Lee-Yang-Parr functional. In DFT, electron density is used to determine the ground state with the help of functionals. B3LYP is the functional is in conjecture with DFT in this study and relies on the Becke 88 exchange functional and the Lee, Yang and Parr correlation functionals. This functional is a hybrid functional since it takes into account the exact exchange of Hartree-Fock theory and it is an approximation of the exchange-correlation in DFT. The Kohn-Sham orbitals are used to express the exact energy functional instead of the density in DFT.

Gaussian 09 calculations[11] were performed to confirm experiments. HPCVL[12] provided the nodes for calculations. Gaussview was the program used to prepare each molecule, molecular ion and protonated ion. Calculations were performed on each molecular ion, their neutral counterparts and their protonated counterparts. Indene, 1-phenyl-1-propyne and fluorene did not

have calculations for their protonated counterparts nor their neutral counterparts. Neutral and ion calculations were used to determine the ionization energies and protonated calculations were used to determine the proton affinity. The method and level of theory used was B3LYP/6-311+G(d,p). Moreover, calculations on the ions of indene, 1-phenyl-1-propyne, fluorene and other possible fragments were performed to determine which ion was a fragment in the MIKES experiments performed.

Chapter 3. Radical Cations

Figure 7 shows the structures of all of the molecules studied in this section.

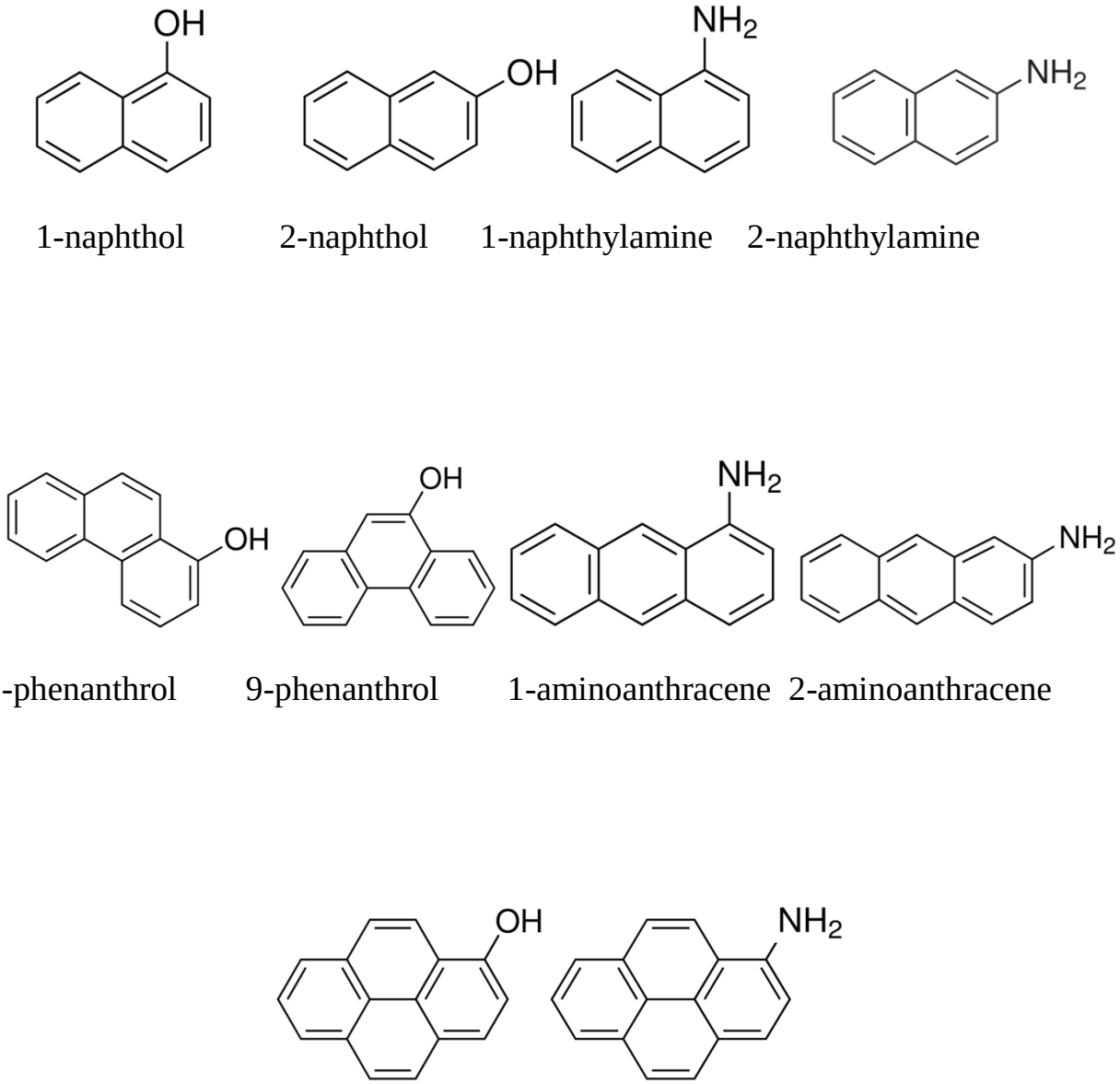

Figure 9: Positional isomers employed in this thesis

Two groups of molecular ions were studied. These two groups are PAHs with different substituents: hydroxy-substituted PAHs and amino-substituted PAHs. Hydroxy- and amino-substituted naphthalenes were studied for the smallest PAH with two rings. There were four of those molecular ions which are 1-naphthol, 2-naphthol, 1-naphthylamine and 2-naphthylamine. To study a trend, bigger PAHs were needed for this study. Thus, a group of PAHs with three rings were studied: 1-phenanthrol, 9-phenanthrol, 1-aminoanthracene and 2-aminoanthracene. Finally, the biggest substituted PAHs studied contained four rings: 1-aminopyrene and 1-hydroxypyrene. The structures of those PAHs are shown in the figure 7. Two positions for the hydroxy groups and amino groups are studied to observe if they have any influence on the ion chemistry of those molecular ions. This discussion is divided to explain the ion chemistry of the hydroxy-substituted PAHs and amino-substituted PAHs separately.

3.1 –OH substituted PAHs

3.1.1 MIKES spectra

MIKES experiments were performed for five hydroxy-substituted PAHs. Two of those PAHs have two aromatic rings: 1-naphthol and 2-naphthol. (Figure 10, 11) They are constitutional isomers of the other, meaning the hydroxy groups are either on the *alpha* position or *beta* position. Two of these PAHs have three aromatic rings: 1-phenanthrol and 9-phenanthrol. Like the substituted naphthalene, the hydroxy-substituted phenanthrenes are molecular ions that are also constitutional isomers of each other and the position of their hydroxy group differs by the one position and nine position. The last group of PAHs studied consisted of four aromatic rings – substituted pyrene. Only one hydroxy-substituted pyrene was studied since no other constitutional isomer was available for purchase.

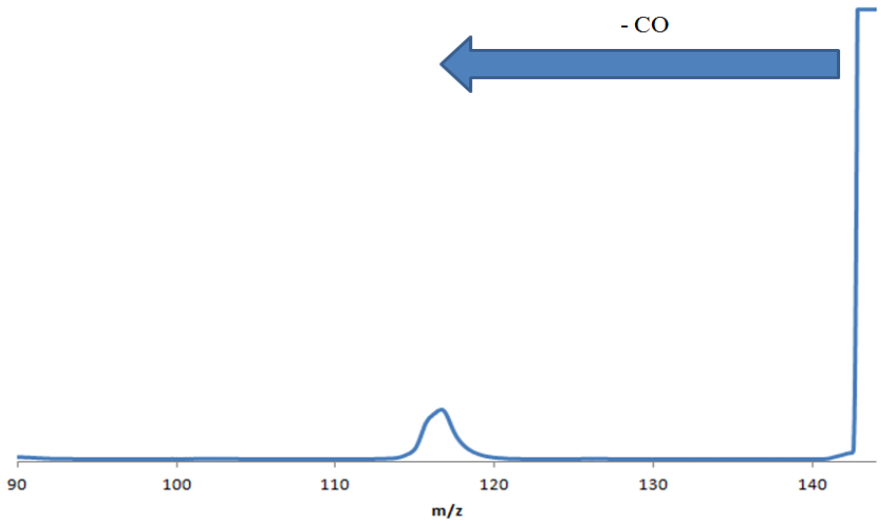

Figure 10: MIKES mass spectra of the 1-naphthol ion m/z 144 (shown cut off to emphasis the product ions). The mass spectrum in blue is at 8 keV.

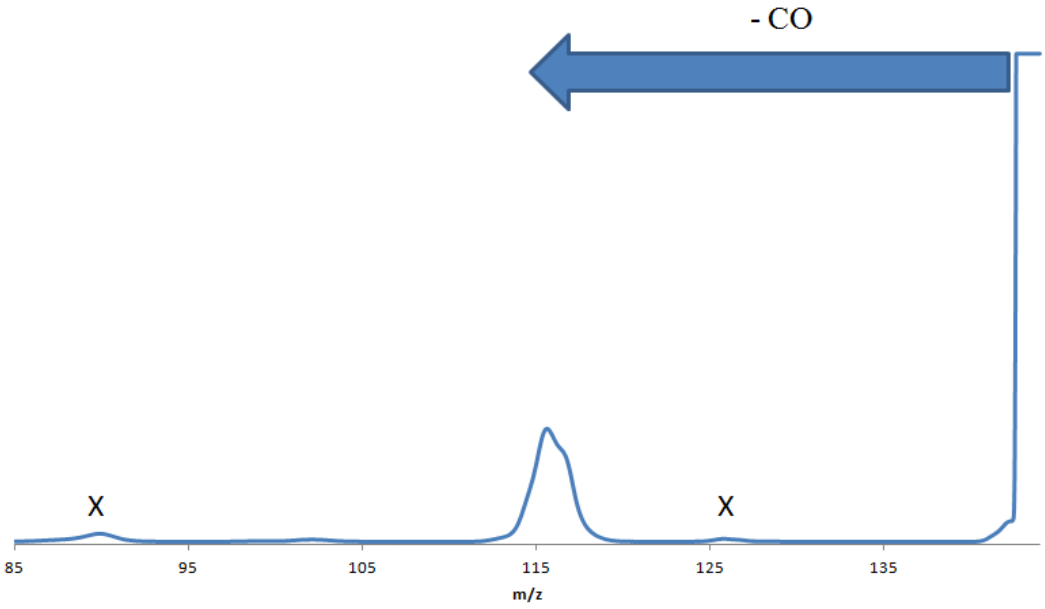

Figure 11: MIKES spectra of 2-naphthol after selecting the parent ion (144 m/z). The spectrum in blue is at 8 keV. (X) refers to collisional artifacts.

Molecular ions that were hydroxy-substituted were found to always lose a neutral fragment of 28 mass units. (Figure 12-14) The neutral compound was found to be carbon monoxide. The fragment ion was found to always be a closed-ring structure and evidence is provided later in this section.

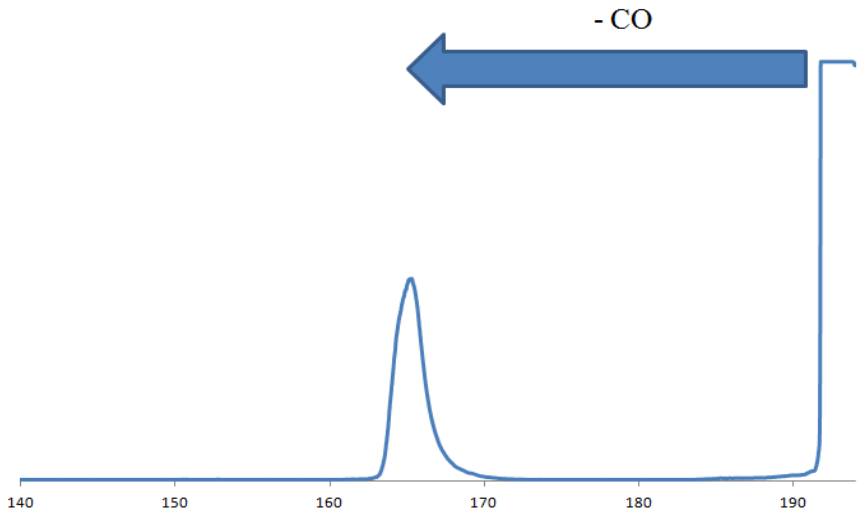

Figure 12: MIKES spectra of 1-phenanthrol after selecting the parent ion (194 m/z). The spectrum in blue is at 8 keV.

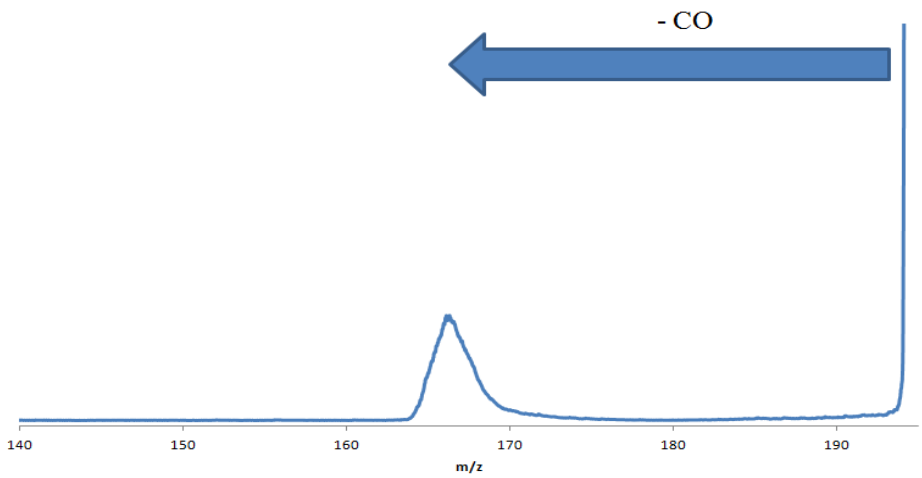

Figure 13: MIKES spectra of 9-phenanthrol after selecting the parent ion (194 m/z). The spectrum in blue is at 8 keV.

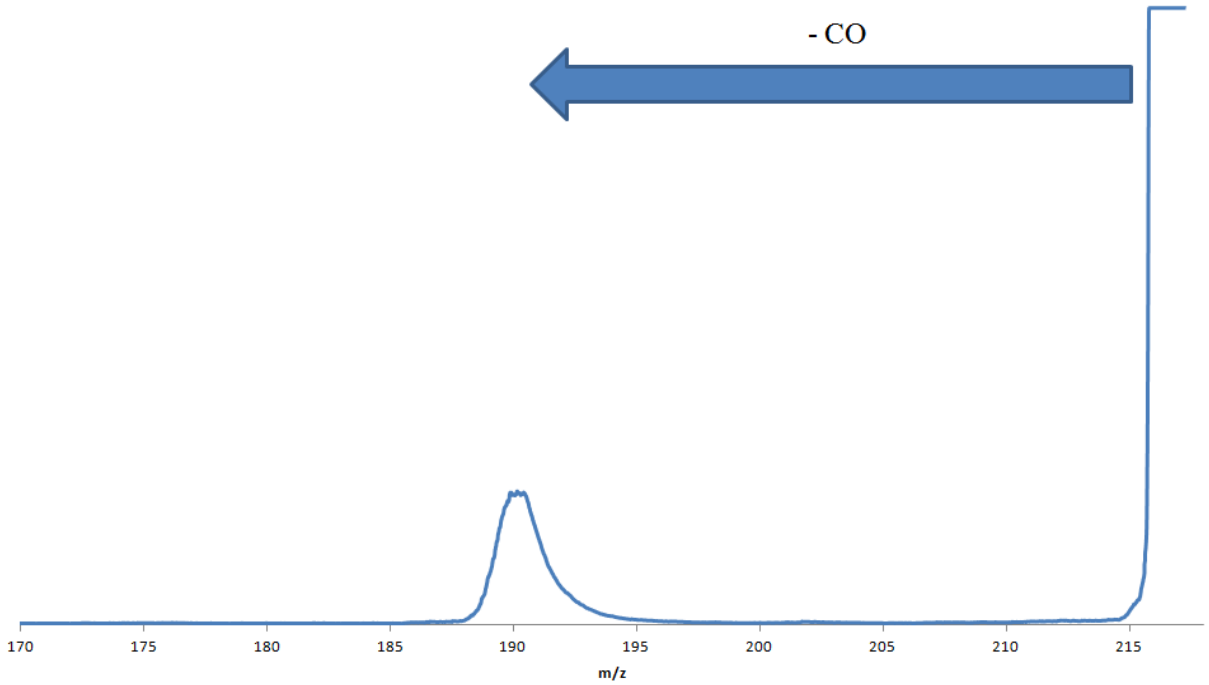

Figure 14: MIKES spectra of 1-hydroxypyrene after selecting the parent ion (218 m/z). The spectrum in blue is at 8 keV.

3.1.2 MI/CID spectra

The MI/CID spectra of all hydroxy-substituted PAHs were collected using helium as a collision gas with 10% beam reduction. MI/CID is used to study the fragmentation pattern of the fragment ion and compare it with the CID spectra of the speculated fragment ion. For hydroxy-substituted naphthalenes, the two speculated fragment ions were indene and 1-phenyl-1-propyne ($C_9H_8^{+\cdot}$). The MI/CID spectra for 1-naphthol and 2-naphthol are shown below:

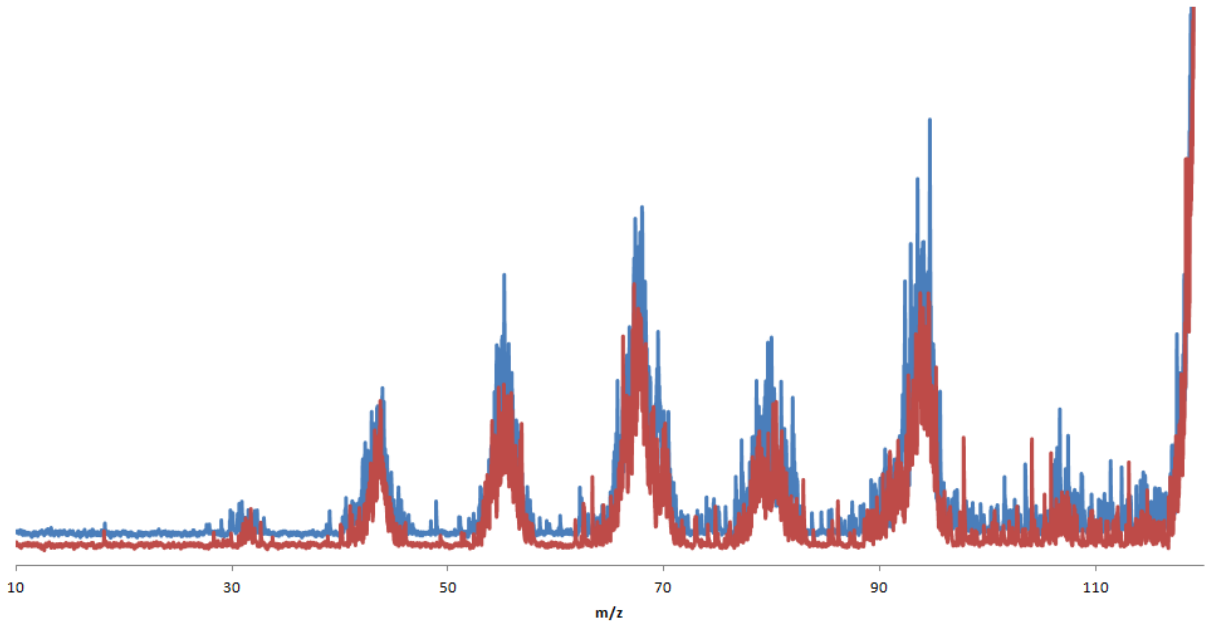

Figure 15: MI/CID spectra of 1-naphthol, in red, and 2-naphthol, in blue, after selecting the fragment ion at 116 m/z

This is to determine which of indene or 1-phenyl-1-propyne is the fragment ion for each molecule. The CID spectra of indene and 1-phenyl-1-propyne are shown below:

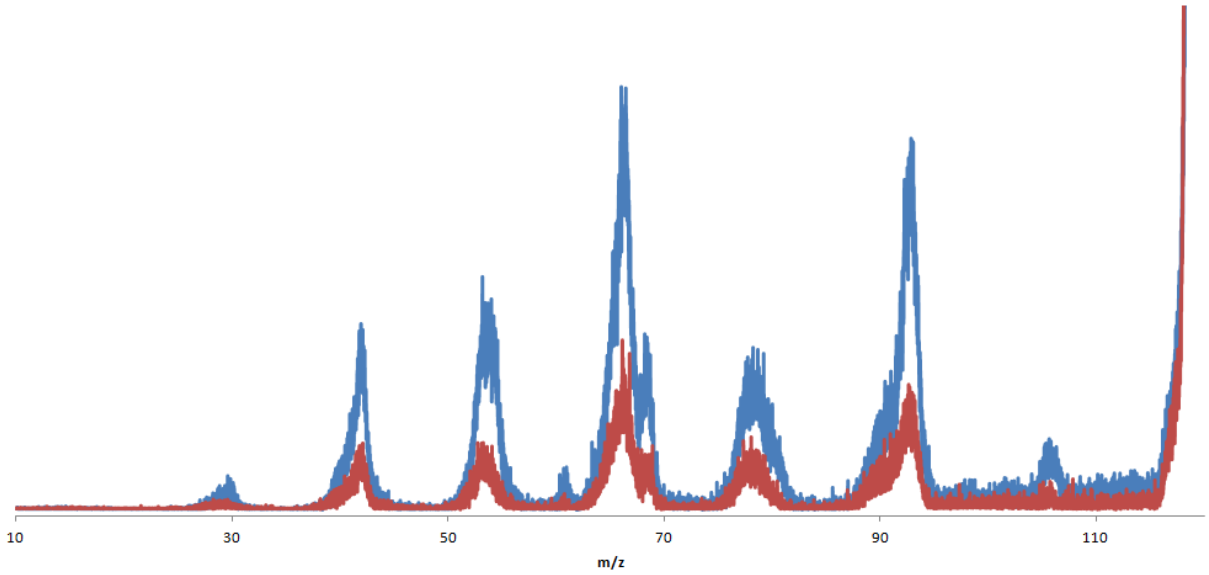

Figure 16: CID spectra of 1-phenyl-1-propyne, in blue, and indene, in red, after selecting the parent ion for each at 116 m/z

As shown with the MI/CID spectra of each naphthol (Figure 15), the spectra are identical. This observation means that the fragment ion for 1-naphthol and 2-naphthol are the same. To determine the ion structure for m/z 116, the MI/CID mass spectra were compared to the CID spectra of ionized indene and 1-phenyl-1-propyne (Figure 16), the two speculated fragment ions of the naphthols. Those results are discussed further on in this thesis.

As for 1-phenanthrol and 9-phenanthrol, the speculated fragment ions were closed-ring structures. However, the only available molecule for purchase for the CID was fluorene, the speculated fragment ion of 9-phenanthrol. As a result, the MI/CID spectra of 1-phenanthrol was

compared to the CID mass spectrum of fluorene in figure 17 and 18. The MI/CID spectrum of 9-phenanthrol compared to the CID spectrum of fluorene is explained further in figure 18. All three spectra are similar and help confirm that the speculated fragment ions are closed-ring structures.

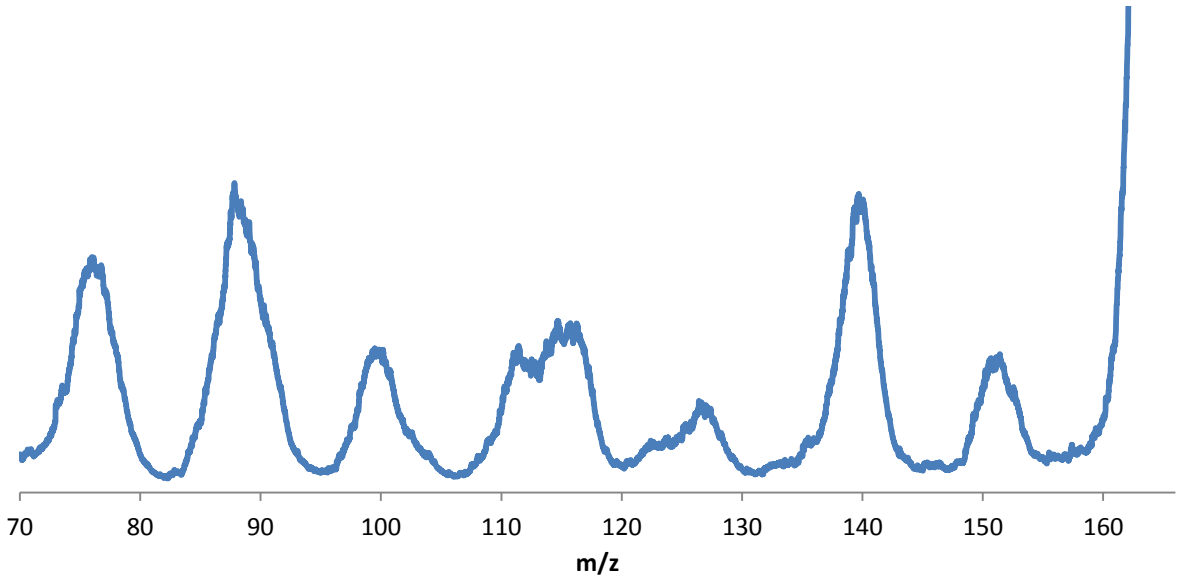

Figure 17: MI/CID spectrum for 1-phenanthrol after selecting the fragment ion at 166 m/z

For 9-phenanthrol, collecting an adequate MI/CID spectrum was challenging. To compare this spectrum with the CID spectrum of fluorene, the MI/CID was not taken into account. This is because the MI/CID of 9-phenanthrol gave the same pattern as the CID of fluorene, but with different peak ratios. With this observation, it was impossible to affirm that the fragment ion 9-phenanthrol was a mix of multiple fragments or only fluorene. The strategy to overcome this problem was to take the CID spectrum for fluorene the same way as usual but to change how the spectrum collected for 9-phenanthrol was taken. For comparison purposes, instead of collecting the MI/CID of 9-phenanthrol, the CID spectra of the fragment ion was

collected from the source. This means that the energy pattern of the fragment ion of 9-phenanthrol and fluorene are similar since both CID spectra are taken in the same conditions. By overlapping each spectra, the fragmentation pattern is as follows:

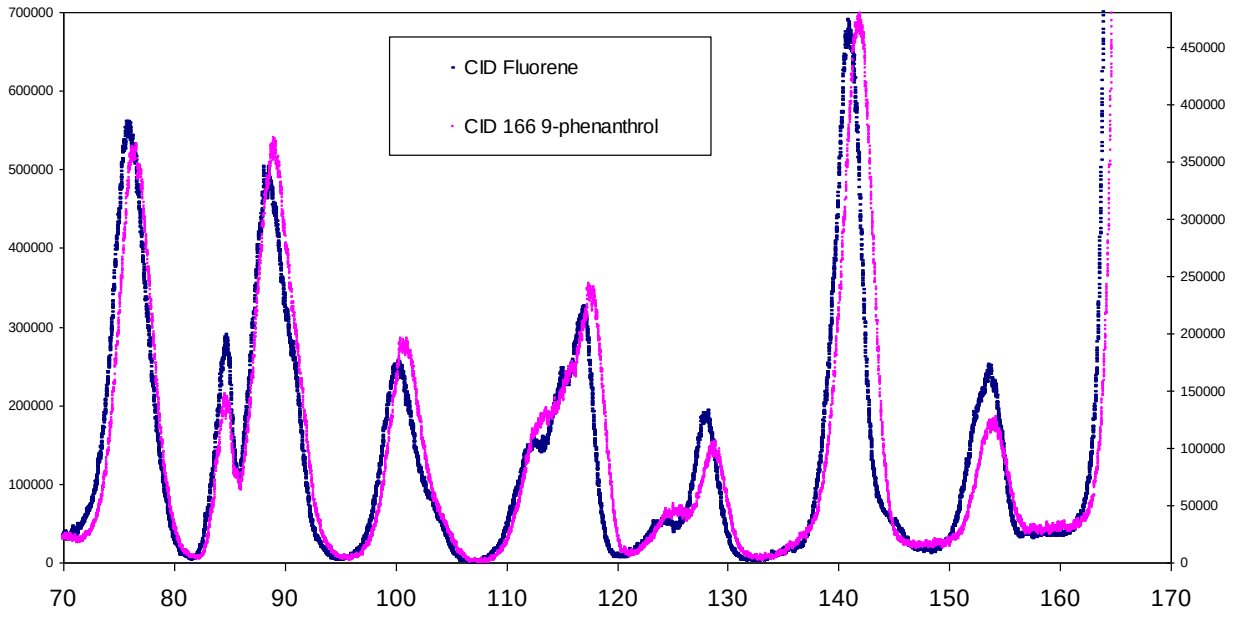

Figure 18: CID spectrum of fluorene in blue and CID spectrum of 9-phenanthrol when selecting directly 166 m/z from the source in pink

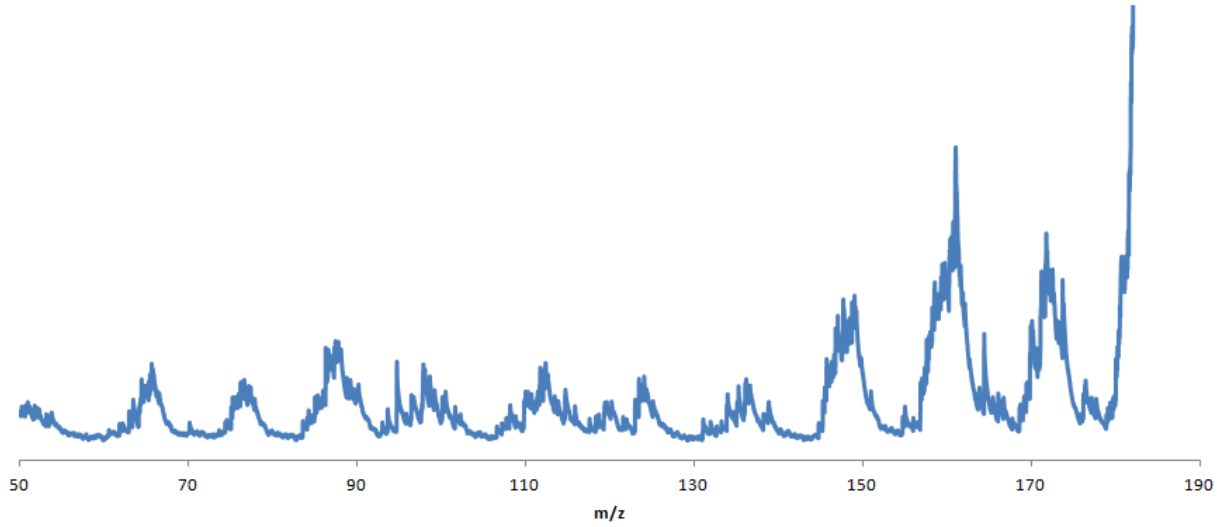

Figure 19: MI/CID spectrum of 1-hydroxypyrene after selecting the fragment ion at 190 m/z

Finally, the MI/CID spectrum for 1-hydroxypyrene was collected. However, the same scenario applies in this case as for 1-phenanthrol. The speculated closed-ring structure for the fragment ion was not available for purchase.

3.1.3 CID spectra

The CID spectra of indene and 1-phenyl-1-propyne were collected using helium as a collision gas with 10% beam reduction. The purpose of this experiment is to compare the CID spectra of indene and 1-phenyl-1-propyne to the MI/CID spectra of 1-naphthol and 2-naphthol.

The CID spectra of indene and 1-phenyl-1-propyne are indistinguishable and are shown in figure 15 and 16. This means that indene and 1-phenyl-1-propyne fragment in the same way. Since their fragmentation pattern is the same, further experiments are needed to determine whether indene or 1-phenyl-1-propyne is the fragment ion for 1-naphthol and 2-naphthol.

3.1.4 Calculation results

The difference in energy between indene and 1-phenyl-1-propyne was calculated using Gaussian 09. The calculations were performed at the B3LYP/6-311+G(d,p) level. Indene is more stable in energy than 1-phenyl-1-propyne by 1.24 eV. These calculations help to confirm that the fragment ion loss is indene, a closed-ring structure.

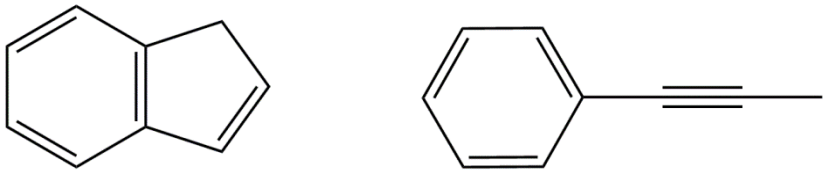

Figure 20: Structure of indene (left) and 1-phenyl-1-propyne (right).

In the case of the hydroxy-substituted phenanthrenes, the method used for calculations was the same as for the hydroxy-substituted naphthalenes. Energies for closed-ring structures and open-ring structures for the fragment ion of 1-phenanthrol and 9-phenanthrol were calculated, although for these cases, every open-ring structure gave a closed-ring calculated structure. This means that the fragment prefers to remain a closed-ring structure over an open-ring structure.

Many different open-ring and closed-ring starting structures were tried for calculations for 1-hydroxypyrene, each time resulting in a closed-ring structure. Again, this means that the closed-ring structure is preferred for the fragment ion loss of 1-hydroxypyrene since this fragment ion prefers to remain a closed-ring structure over an open-ring structure.

3.1.5 Mechanisms

In the dissociation, internal energy of the precursor ion is converted into the relative translational energy of the products, a process that is called "kinetic energy release". If this release, which can occur in all directions, is large, then ions having a large component of this in the z-axis direction of the instrument can miss the entrance of the ESA, causing a depression in signal at the centre of the beam (z-axial discrimination). The result is a dish-shaped peak. A large kinetic energy release is common if the dissociation occurs on a potential energy surface that has a large reverse activation barrier. The internal energy of the products tends to be statistically distributed between translational, rotational and vibrational modes of the products, the dish-shaped peak being the observable products of the translational portion of this process. A large reverse activation barrier is usually indicative of a intra-molecular rearrangement process that takes place prior to dissociation. Thus, naphthol ions undergo rearrangement before losing neutral carbon monoxide. Figures 21-25 shows possible mechanisms based on previously reported mechanisms for CO loss from ionized phenol.[13 14]

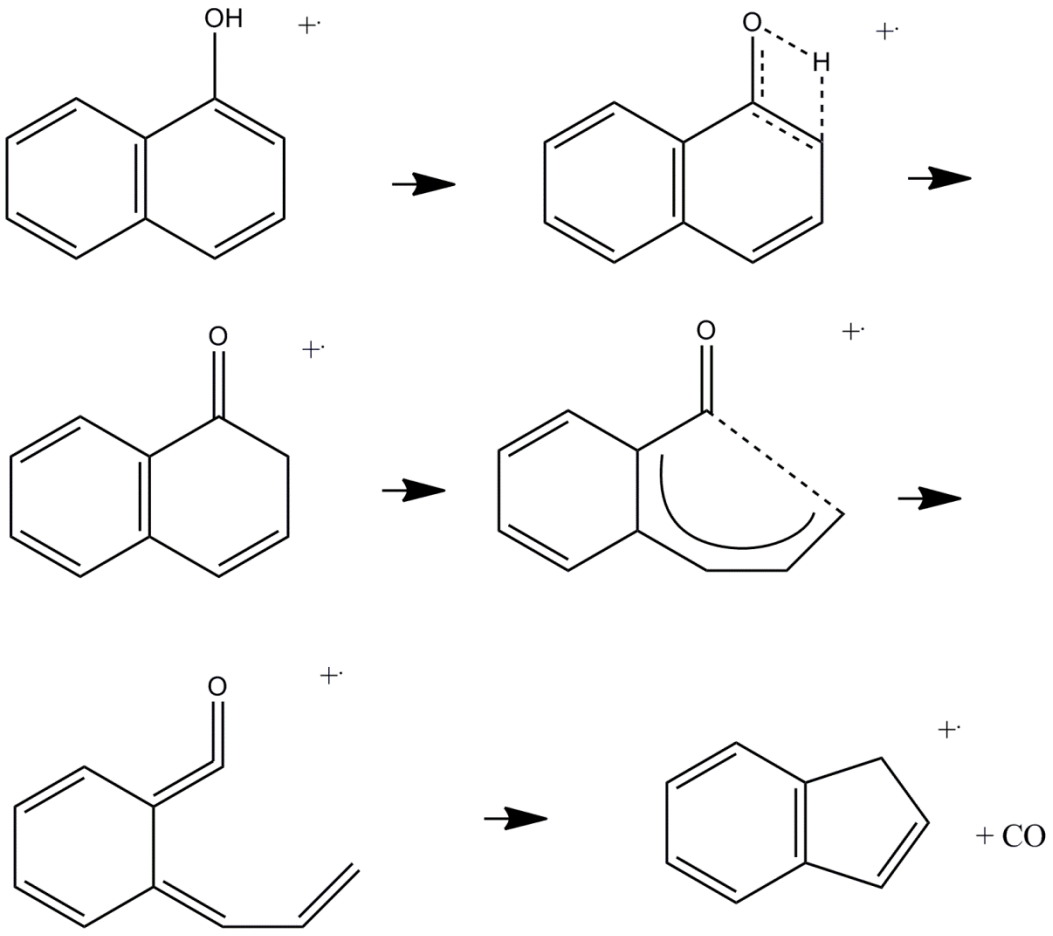

Figure 21: Proposed mechanism for the loss of CO for 1-naphthol

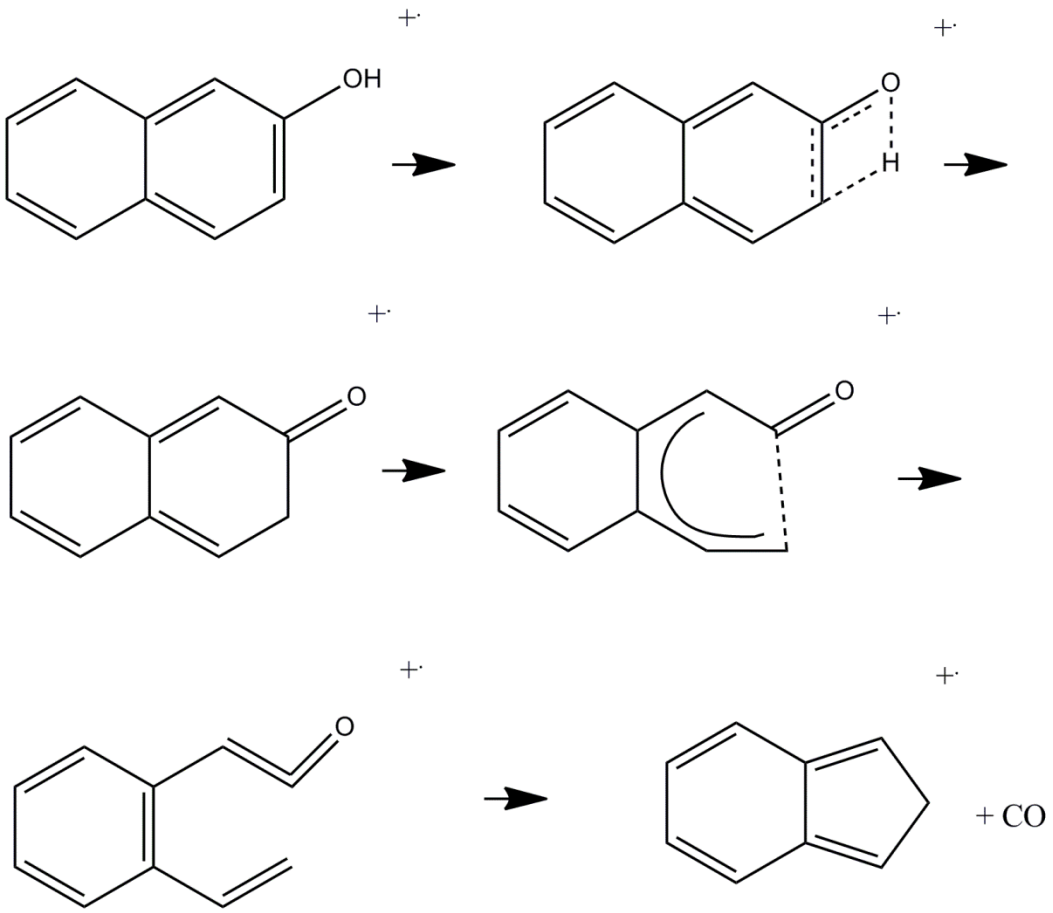

Figure 22: Proposed mechanism for the loss of CO for 2-naphthol

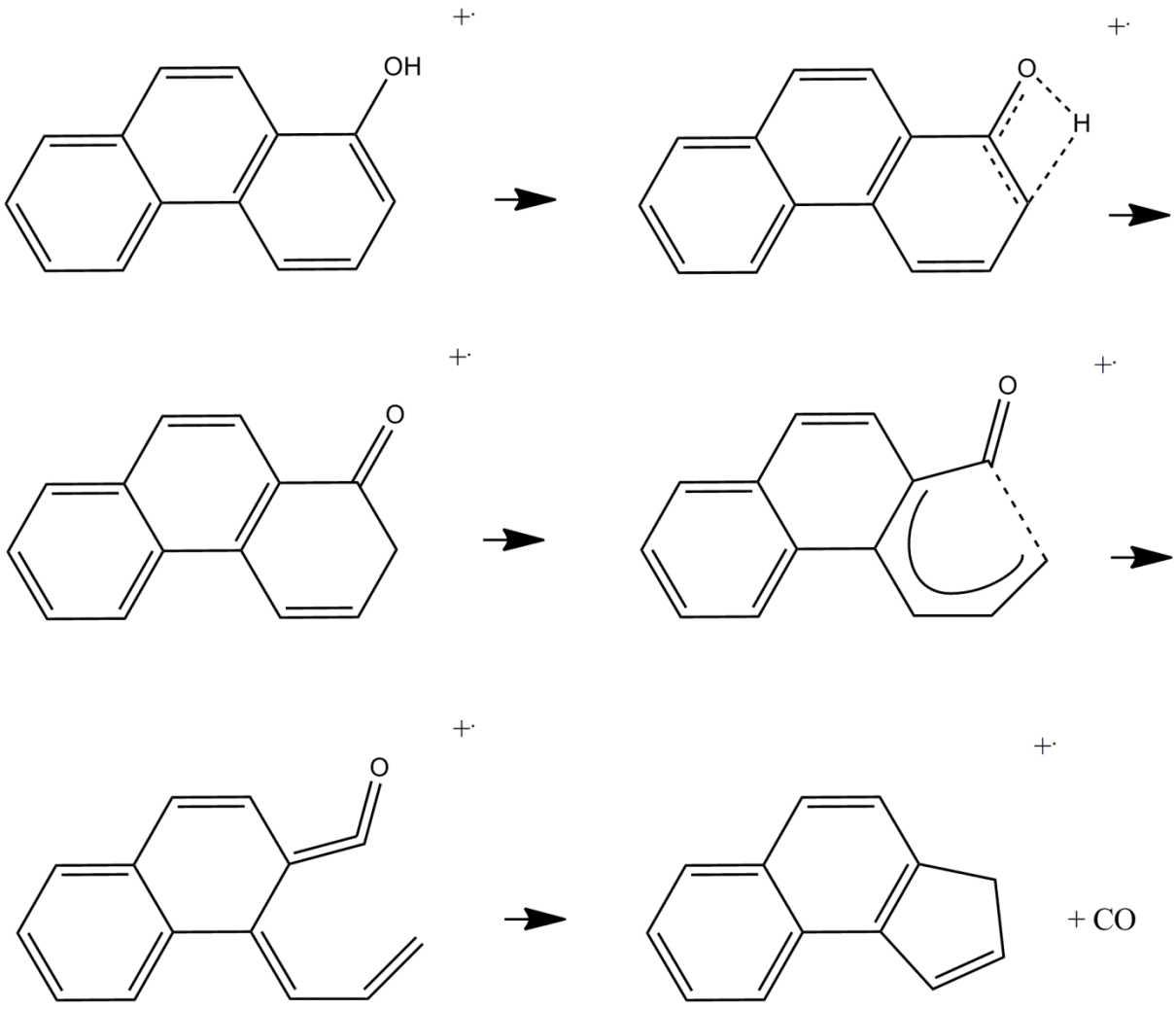

Figure 23: Proposed mechanism for the loss of CO for 1-phenanthrol

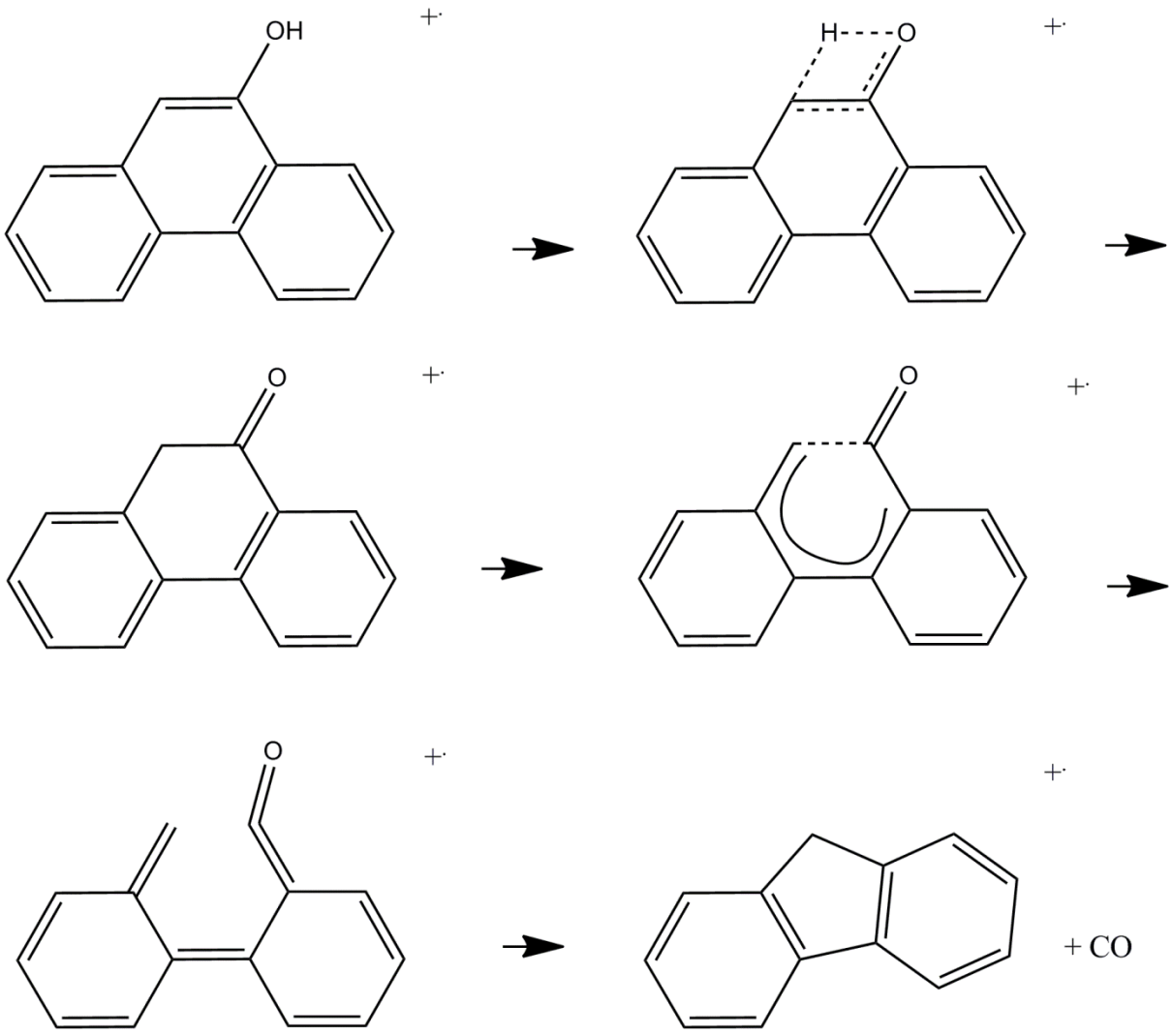

Figure 24: Proposed mechanism for the loss of CO for 9-phenanthrol

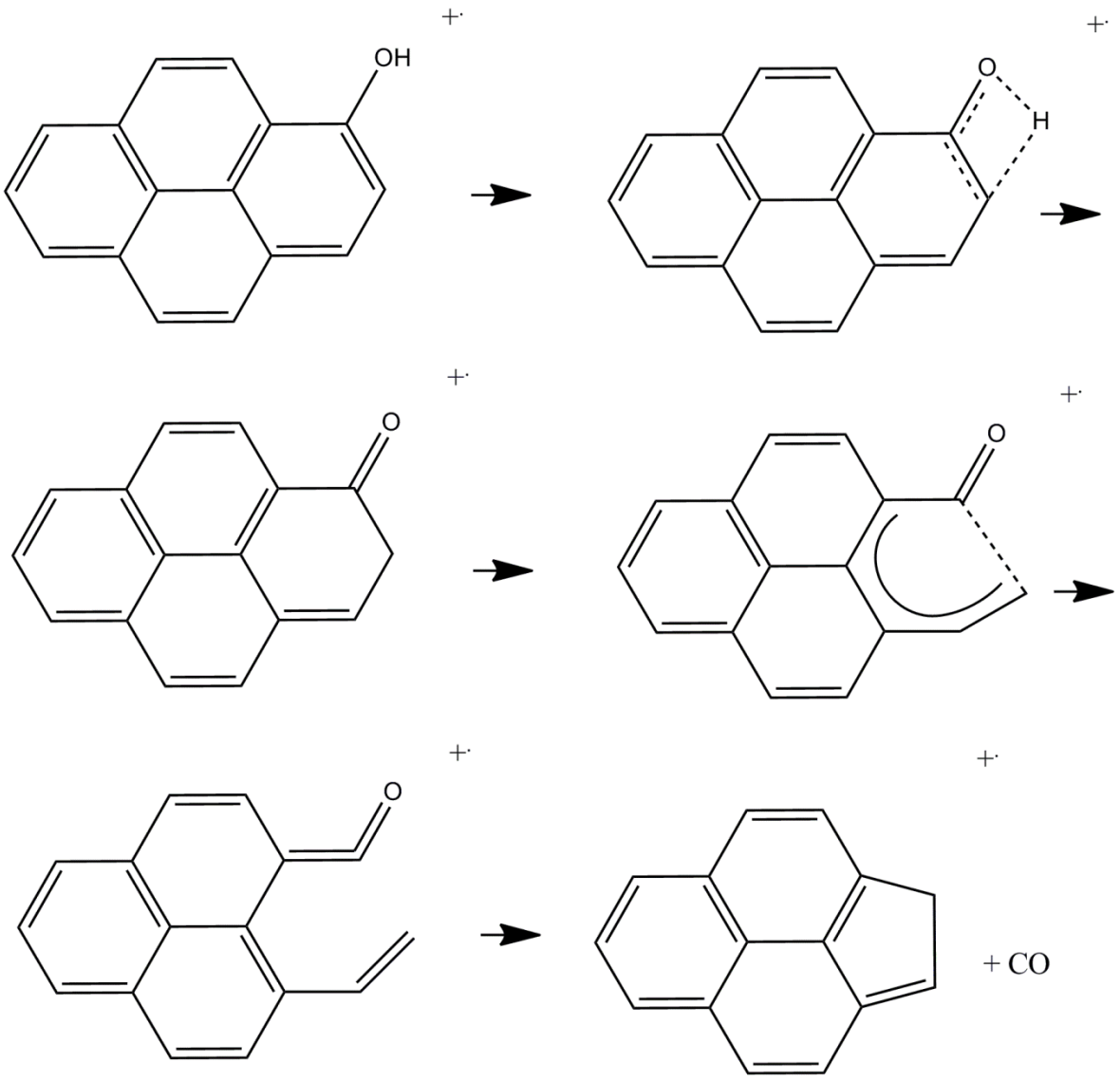

Figure 25: Proposed mechanism for the loss of CO for 1-hydroxypyrene

3.1.6 Extrapolation to larger PAHs

In the interstellar medium, PAHs are speculated to be of at least 50 carbons. The findings on the hydroxy-substituted PAHs serve to be extrapolated to these bigger PAHs. By extrapolating, the bigger PAHs in the interstellar medium would lose carbon monoxide and the

fragment ion would be a closed-ring structure. This can be speculated by using the proposed mechanisms and extrapolating them to bigger PAHs. These mechanisms always lead to a closed-ring product and always lead to a loss of carbon monoxide. As for the calculations, the same speculation can be established since every speculated structure rearranged to give a closed-ring structure. Finally, calculations, proposed mechanisms and MI/CID spectra go hand-in-hand and predict a loss of carbon monoxide for hydroxy-substituted PAHs with a remaining closed-ring structure for PAHs of 50 carbons or more that are speculated to be present in the interstellar medium.

3.2 $-NH_2$ substituted PAHs

3.2.1 MIKES spectra

MIKES data were collected for five amino-substituted PAHs. Two of those PAHs have two aromatic rings: 1-naphthylamine and 2-naphthylamine. They are constitutional isomers of the other, meaning the amino groups are either on the *alpha* position or *beta* position. Two of those PAHs have three aromatic rings: 1-aminoanthracene and 2-aminoanthracene. Like the substituted naphthalene, the amino-substituted anthracenes are molecular ions that are also constitutional isomers of each other and the position of their amino group differs by the one position and two position. The last group of PAHs studied consisted of four aromatic rings – substituted pyrene. Only one amino-substituted pyrene was studied since no other constitutional isomer was available for purchase.

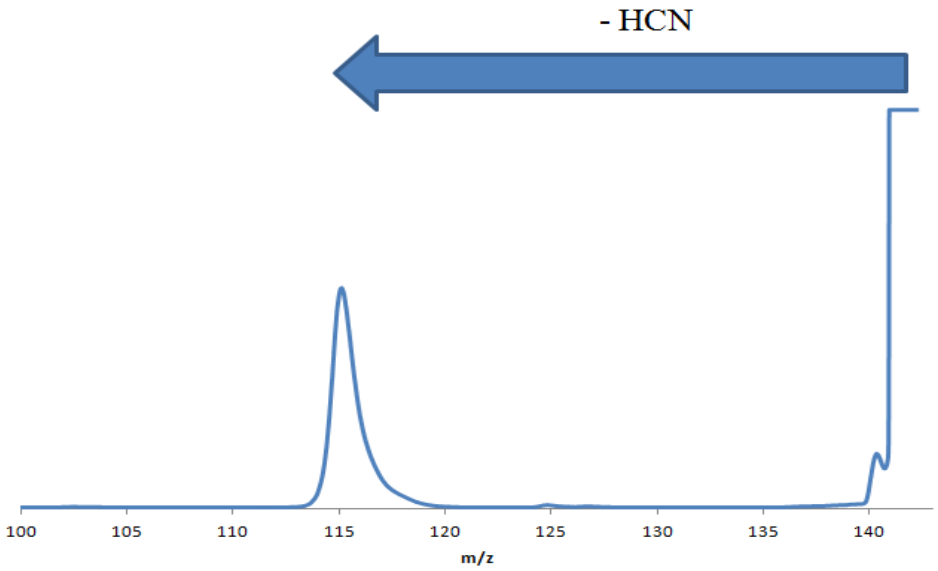

Figure 26: MIKES spectra of 1-naphthylamine after selecting the parent ion (143 m/z). The spectrum in blue is at 8 keV. Some H loss was also observed.

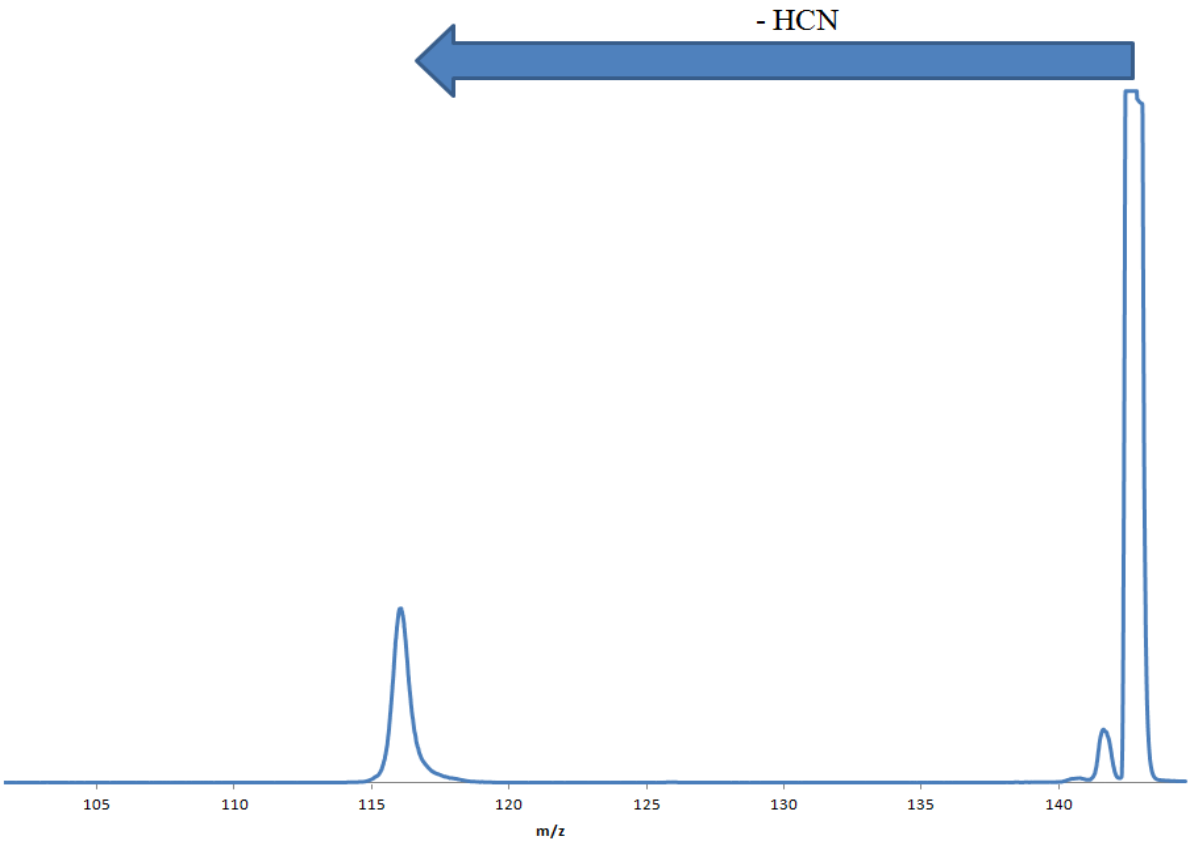

Figure 27: MIKES spectra of 2-naphthylamine after selecting the parent ion (143 m/z). The spectrum in blue is at 8 keV. Some H loss is also observed.

Molecular ions that were amino-substituted were found to always lose a neutral fragment of 27 (presumably HCN as it is significantly more stable than HCN). Some H loss was also observed. Since the fragmentation pattern of the MI/CID of both naphthylamines are the same as the fragmentation patter of the MI/CID of both naphthols, HCN is the neutral compound loss and not C_2H_3 (see figure 15, 16 and 30) as the product ion is consistent with the indene/phenylacetylene structure. The resulting fragment ion is at the same mass as the hydroxy-substituted counterparts. For the amino- and hydroxy-substituted naphthalene molecular ions, the fragment ion is found to always have a 116 m/z.

The peak at 116 m/z for the amino substituted naphthalene was of a Gaussian shape unlike hydroxy-substituted PAHs.

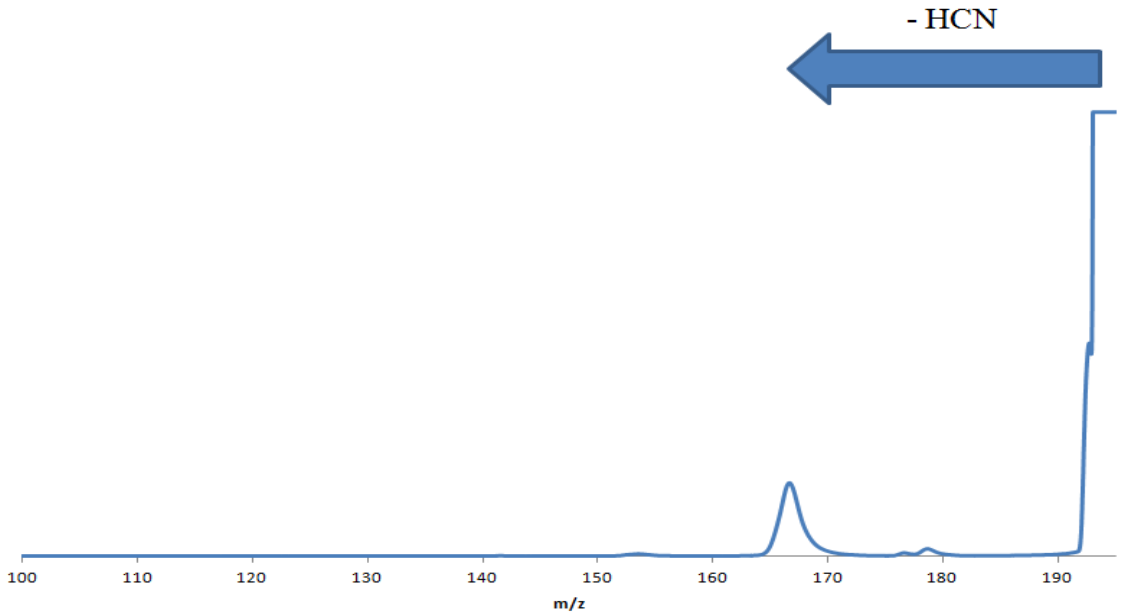

Figure 28: MIKES spectra of 1-aminoanthracene after selecting the parent ion (193 m/z). The spectrum in blue is at 8 keV.

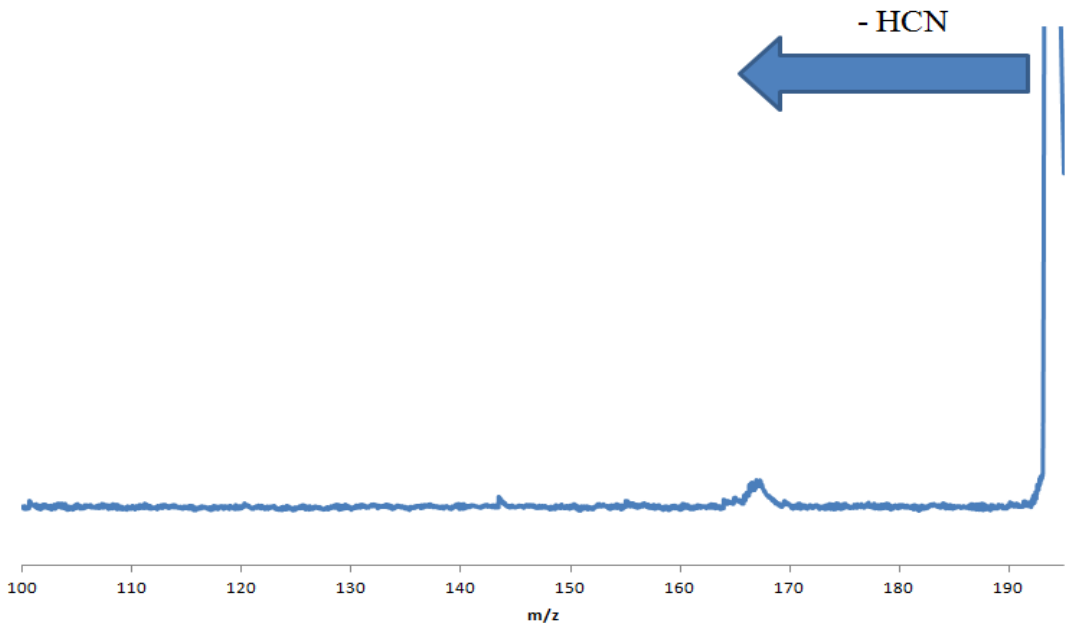

Figure 29: MIKES spectra of 2-aminoanthracene after selecting the parent ion (193 m/z). The spectrum in blue is at 8 keV.

3.2.2 MI/CID spectra

The MI/CID spectra of 1-naphthylamine and 2-naphthylamine were collected to determine whether indene or 1-phenyl-1-propyne was the fragment ion in each case by comparing them with the CID spectra for indene and 1-phenyl-1-propyne. The MI/CID spectra of 1-naphthylamine and 2-naphthylamine were collected using helium as a collision gas with 10% beam reduction. The MI/CID spectra of 1-naphthylamine and 2-naphthylamine are shown below:

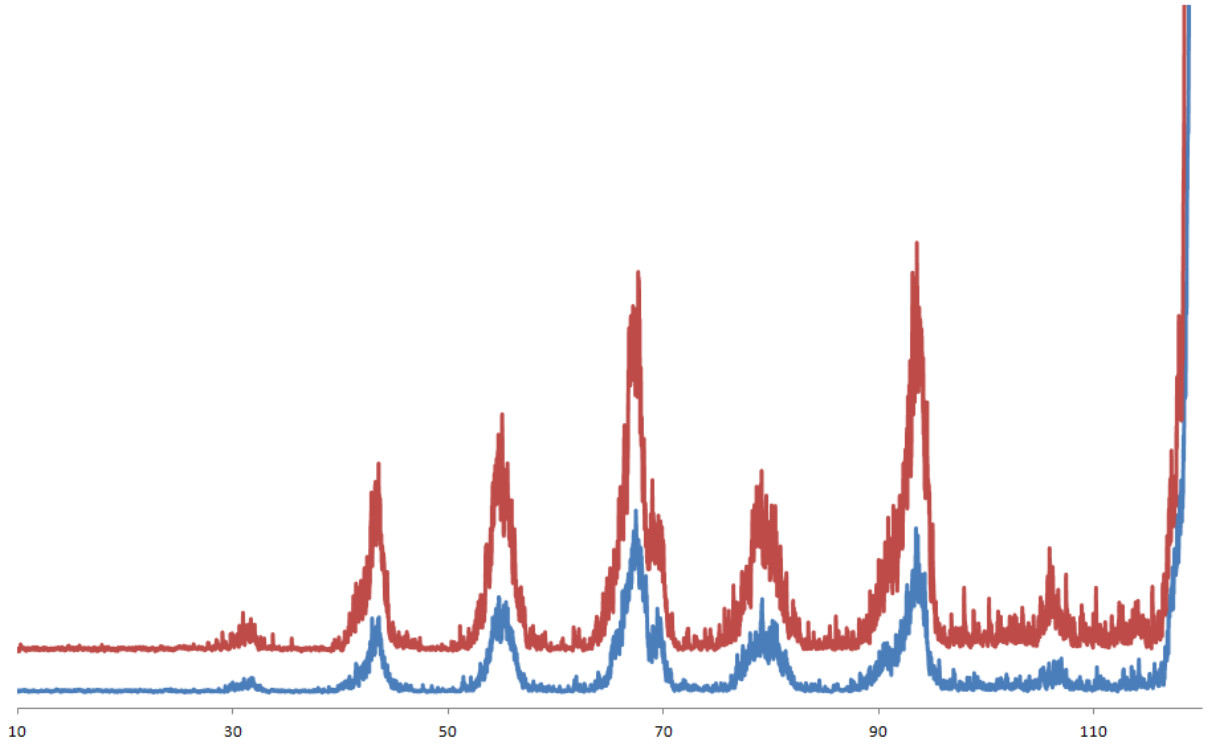

Figure 30: MI/CID spectra of 1-naphthylamine, in blue, and 2-naphthylamine, in red, after selecting the fragment ion at 116 m/z

The scenario in this case is the same as for the naphthols: the spectra are identical. Again, this means that the fragment ion for 1-naphthylamine and 2-naphthylamine are the same. Since the two speculated fragment ions of the naphthylamines are indene and 1-phenyl-1-propyne, determining which molecule the fragment ion is using the MI/CID spectra of each naphthylamine by comparing them to the CID spectra of indene and 1-phenyl-1-propyne would help distinguish them. As discussed earlier, the CID spectra of indene and 1-phenyl-1-propyne are indistinguishable (figure 17) and thus we have to rely on calculations to conclude that indene was the more stable product ion and thus the one most likely to be produced. It is then possible

to conclude that the substituent does not matter and that indene is always the fragment ion for both the naphthols and the naphthylamines.

As for the remaining amino-substituted PAHs, the speculated structure for each fragment ion was not purchasable. Even then, the spectra were collected for 1-aminoanthracene, 2-aminoanthracene and 1-aminopyrene. The spectra are shown below:

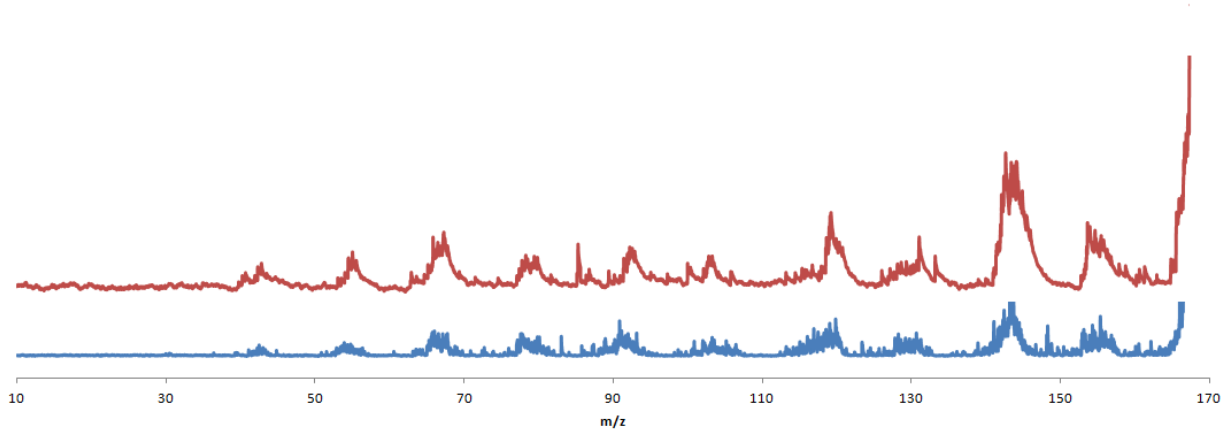

Figure 31: MI/CID spectra of 2-aminoanthracene, in red, and 1-aminoanthracene, in blue, after selecting the fragment ion at 166 m/z

3.2.3 CID spectra

These experiments were important to perform on indene and 1-phenyl-1-propyne to determine if they were the resulting fragments in the MIKES spectra of 1-naphthylamine and 2-

naphthylamine. The figure comparing indene and 1-phenyl-1-propyne were presented earlier in figure 16. As stated previously, the CID spectra for indene and 1-phenyl-1-propyne are the same. Thus, the two structures are indistinguishable.

3.2.4 Calculation results

All amino-substituted PAHs lose HCN and the fragment ion is always a closed-ring structure for every molecular ion. This can be explained by calculating the energy of a closed-ring structure versus an open-ring structure. The two possibilities for the amino-substituted naphthalenes were the same as for the hydroxy-substituted naphthalenes. Indene was the possibility for a closed-ring structure and 1-phenyl-1-propyne was the possibility for an open-ring structure. As stated earlier, indene is more stable in energy than 1-phenyl-1-propyne by 1.24 eV. These calculations help to confirm that the fragment ion loss is indene, a closed-ring structure. These results mean that the position and the nature of the substituent is not an important factor to obtain indene as a fragment ion. In all cases for substituted naphthalene, the fragment ion was always a closed-ring structure, indene.

In the case of the amino-substituted anthracenes, the method used for calculations was the same as for the amino-substituted naphthalenes. Energies for closed-ring structures and open-ring structures for the fragment ion of 1-aminoanthracene and 2-aminoanthracene were calculated, although for these cases, every open-ring structure gave a closed-ring calculated structure. This means that the fragment prefers to remain a closed-ring structure over an open-

ring structure. Confirmation of these calculations using MI/CID was discussed earlier in this thesis.

Many different open-ring and closed-ring starting structures were tried for calculations for 1-aminopyrene, each time resulting in a closed-ring structure. Again, this means that the closed-ring structure is preferred for the fragment ion loss of 1-aminopyrene since this fragment ion prefers to remain a closed-ring structure over an open-ring structure.

3.2.5 Mechanisms

The speculated rearrangements amino-substituted PAHs undergo are shown below (figures 32-36):

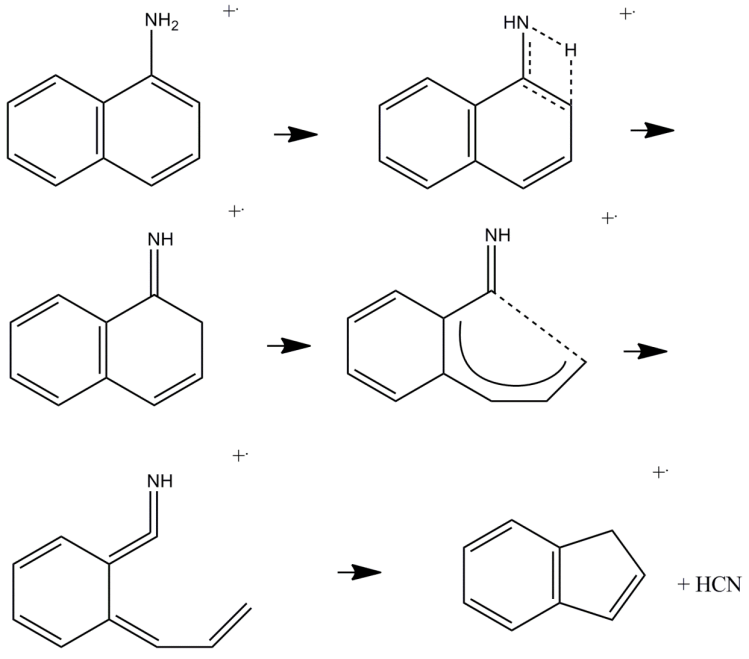

Figure 32: Proposed mechanism for the loss of HCN for 1-naphthylamine

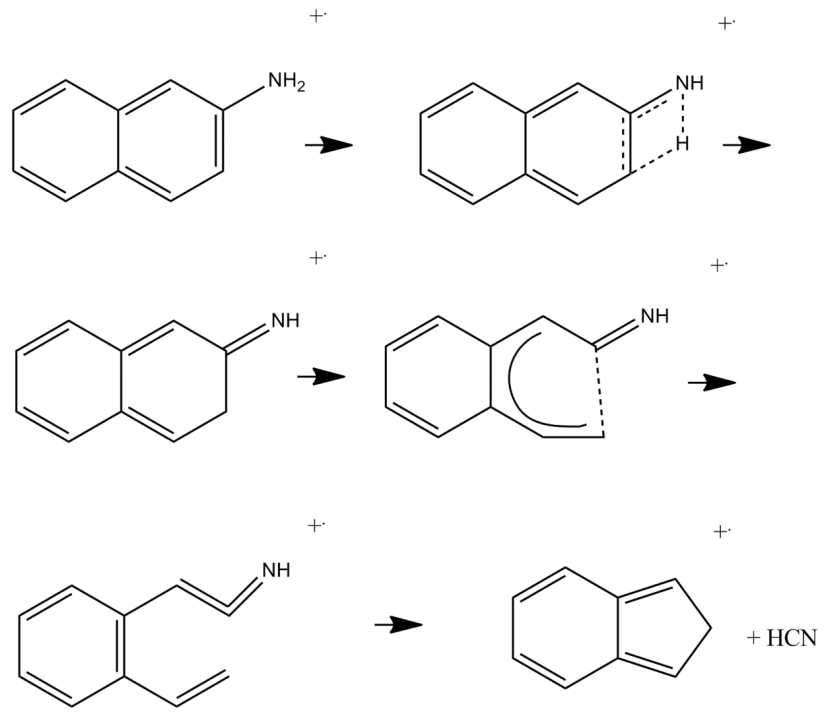

Figure 33: Proposed mechanism for the loss of HCN for 2-naphthylamine

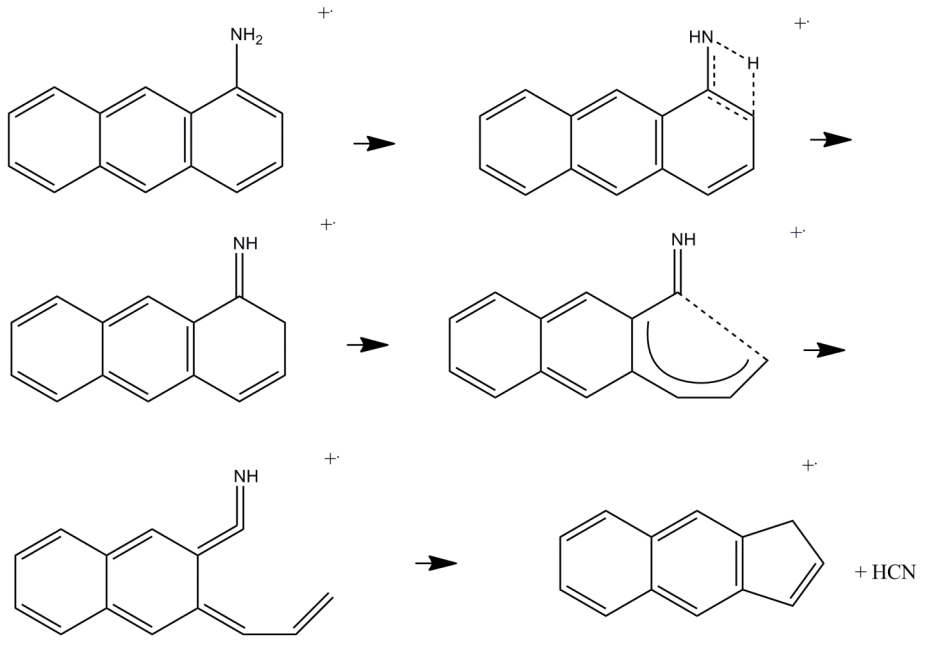

Figure 34: Proposed mechanism for the loss of HCN for 1-aminoanthracene

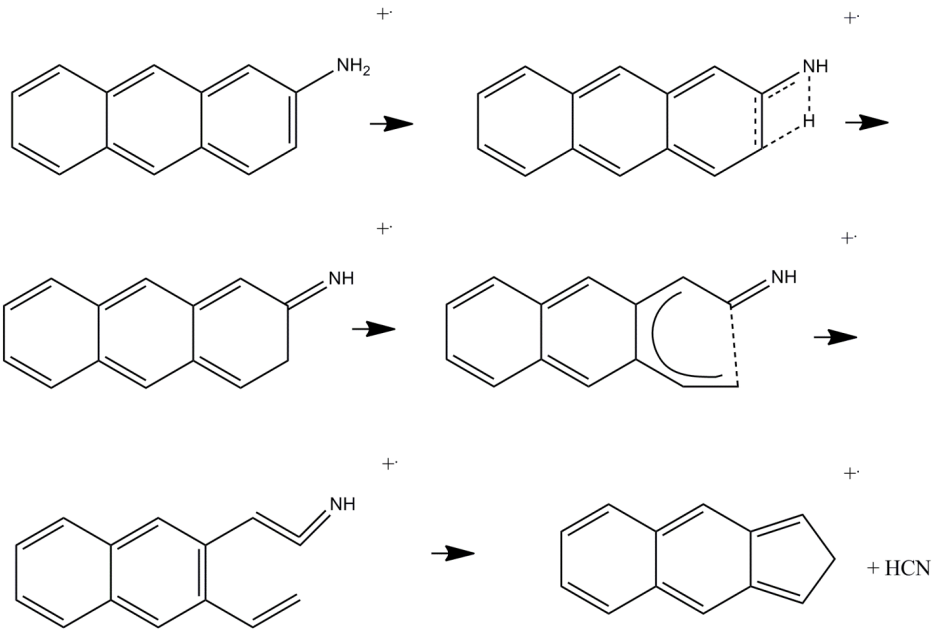

Figure 35: Proposed mechanism for the loss of HCN for 2-aminoanthracene

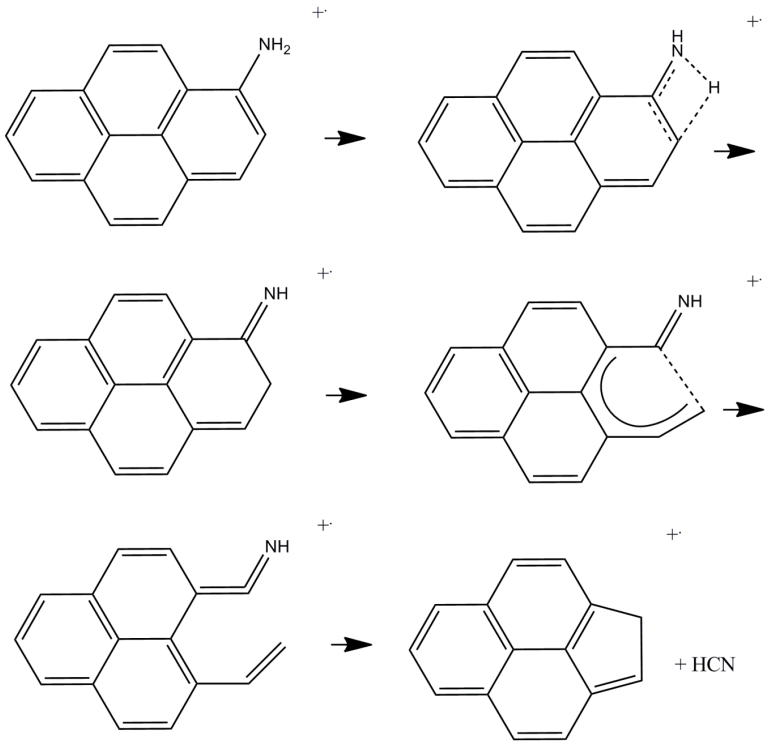

Figure 36: Proposed mechanism for the loss of HCN for 1-aminopyrene

3.2.6 Extrapolation to larger PAHs

Since the interstellar medium is believed to be populated by bigger PAHs of at least 50 carbons, extrapolation is needed. Those bigger PAHs are not possible to study using our setup because their vapor pressure is too low. However, using the results found for the MIKES experiments, extrapolation can be done. If the trend continues, bigger amino-substituted PAHs should also lose 27 m/z which is HCN. The same trend could be seen for the bigger amines, which would always lose 27 m/z which is HCN.

Chapter 4. Protonated PAHs

Protonation of the PAHs studied in this thesis was attempted.[15] [16] [17] [18] The goal was to investigate if the proton would attached to the hydroxy group and amino group to eventually lose water and ammonia. Since the most abundant atom in the universe is hydrogen, the likelihood of one proton finding a PAH to react with is greater than any other possibility. Finding how hydroxy-substituted PAHs and amino-substituted PAHs reacted in presence of such a proton would thus be interesting to investigate. Finding a trend to relate the results to larger PAHs was also investigated and is further detailed later in this thesis.

Some calculations were performed to find the proton affinity of each compound being studied to investigate if protonation was possible in the gas-phase. Calculations were performed before protonating because the proton affinity needed to be investigated to determine if it was worth attempting to protonate. If the proton affinity calculated would let protonation to occur, the experiment to protonate each PAHs using a VG-ZAB and methane would thus begin.

4.1 Calculations

Calculations were performed using the High Performance Computing Virtual Laboratory (HPCVL). The level of theory used for all calculations was B3LYP/6-311+G(d,p) and MP2/6-311+G(d,p). The proton affinity of each molecular ion studied were calculated. The equation used to calculate the proton affinity is as follow:

$$-(MH^{+\cdot} - M^{+\cdot}) = Proton\ affinity$$

Table 1: Proton affinities (eV) of the PAHs studied in this thesis, calculated using two different methods

Molecules	B3LYP	MP2
1-naphthol	**8.10**	**8.06**
2-naphthol	7.83	7.79
1-naphthylamine	**9.17**	9.16
2-naphthylamine	9.15	9.16
1-phenanthrol	**7.88**	**7.80**
9-phenanthrol	7.84	7.78
1-aminoanthracene	**9.25**	9.22
2-aminoanthracene	9.22	9.22
1-hydroxypyrene	7.95	7.85
1-aminopyrene	**9.25**	

Two methods were used for the calculations to ensure the reliability of the DFT calculation. To ensure DFT was reliable, MP2 was used. By looking at the calculated proton affinities, MP2 ensures that DFT is a reliable method of calculation because the numbers given by each calculation are very close.

The results show that for the naphthols, it is easier to protonate 1-naphthol by 0.27 eV, which is a much greater difference in proton affinity than the rest of the compounds when comparing the constitutional isomers.

The calculations showed that 1-hydroxypyrene and 1-aminopyrene were 1.30 eV apart when looking at their proton affinities. As previously mentioned, the amino-substituted counterparts were easier to protonate than the hydroxy-substituted compounds. Again, by calculating the HOMO of the neutral molecule and the protonated molecular ion, the electronic density around the $–H_2O$ was smaller than the one surrounding the $–NH_3$ group. If the trend continues, the observation would be that the proton affinity would increase with the size of the PAH. However, even though bigger PAHs would have a higher proton affinity than smaller PAHs, the proton affinity does not continue to get larger indefinitely.[19] Since the interstellar medium is believed to have bigger PAHs, this trend is important to establish. Protonation would be possible on the bigger alcohols and amines PAHs.

4.2 Protonation of 1-naphthol and 2-naphthol using the VG-ZAB

The protonation of 1-naphthol and 2-naphthol was achieved in a high-pressure source using methane by performing chemical ionization. Two MI processes were observed in the MIKES spectrum of protonated 1-naphthol and 2-naphthol, m/z 145 (Figures 37, 38).

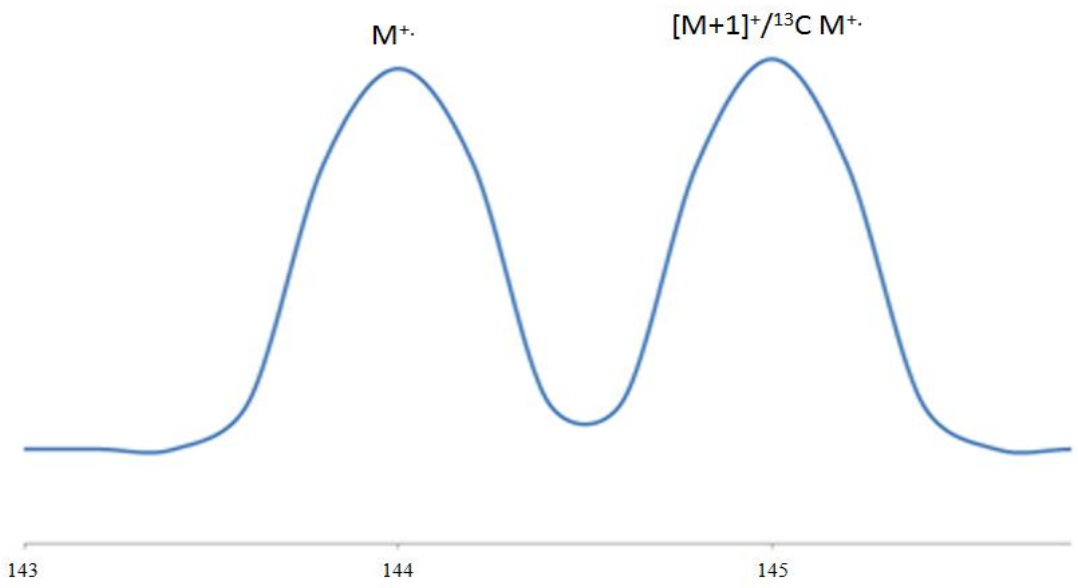

Figure 37: Mass spectrum depicting the relative intensity of the M+1 peak being a mix of $[M+H]^+$ and $^{13}C\ M^{+\cdot}$ and the $M^{+\cdot}$ peak

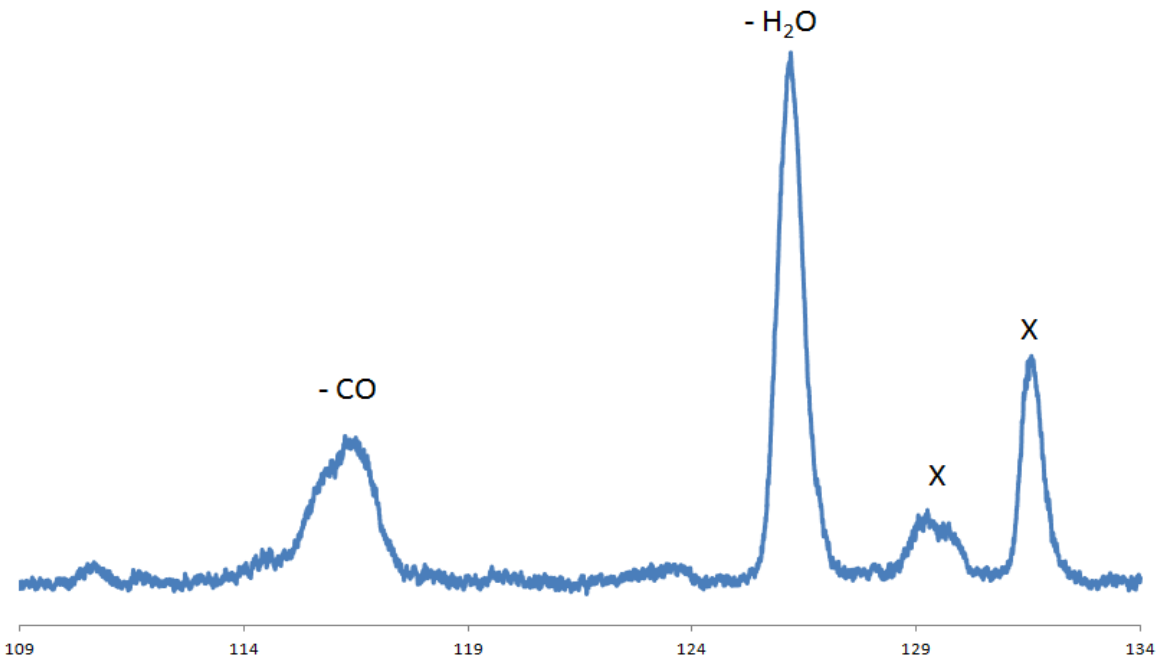

Figure 38: MIKES spectrum of protonated 2-naphthol after selecting m/z 145. (X) shows collisional artifacts

Loss of H_2O and CO are evident. However, it is possible that CO loss is coming from the M+. ion having one ^{13}C atom, which also has m/z 145 and has a relative abundance of 10% of the peak at m/z 144, overlapping the peak for protonated naphthol. (Figure 37) To determine the origin of the CO loss peak, the ratio of the intensity of the H_2O loss vs the CO loss peaks in the MIKES spectra were measured as a function of the relative intensity of $M^{+\cdot}$ at m/z 144 to the peak of m/z 145 (Figures 37-38). As the protonation increases, the loss of H_2O becomes more and more dominant. This means that the CO loss comes exclusively from the carbon-13 contribution of $M^{+\cdot}$ and not from the protonated molecule. This can be explained since loss of water becomes more and more dominant. If carbon monoxide loss came from the protonated

molecule and not from the carbon-13 contribution, the ratio would stay the same for each ratio of M+1 to M. This is clearly not the case in this study. The same trend is observed for the protonation of 2-naphthol. The loss of water becomes more and more dominant as the protonation increases, meaning that CO loss comes again exclusively from the carbon-13 contribution and not from the protonated species.

Protonation was studied using the above process since it was not possible to protonate 1-naphthol and 2-naphthol to the point where their $M^{+\cdot}$ peak would be almost non-existent, making the carbon-13 contribution to m/z 145 meaningless.

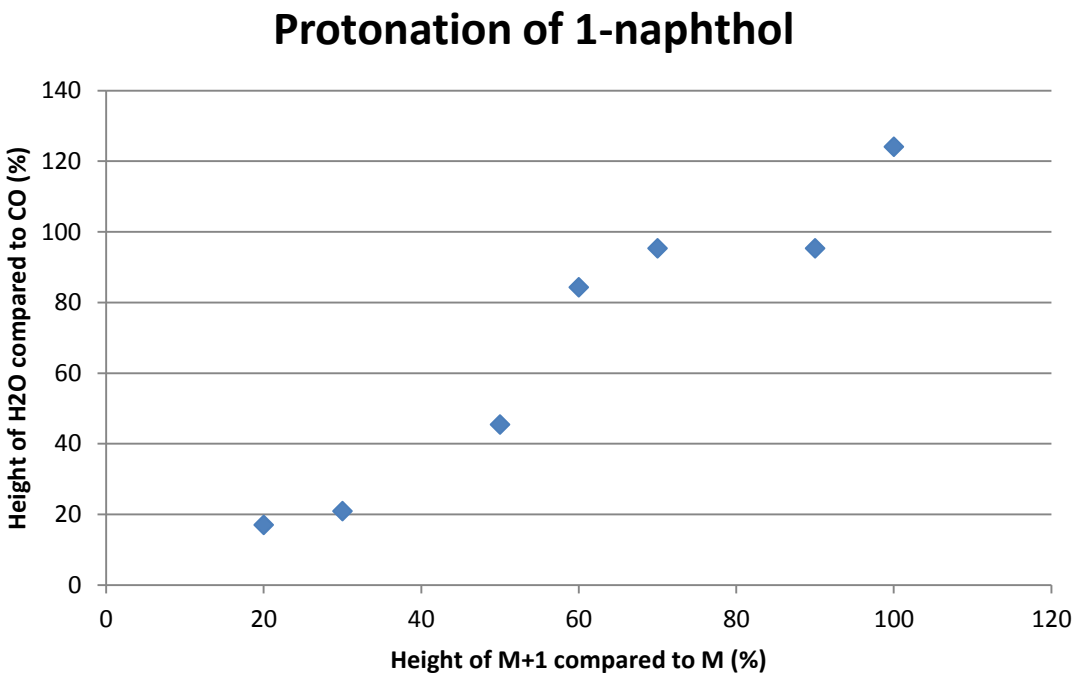

Figure 39: Graph showing the protonation of 1-naphthol using methane as a chemical ionization gas. The ratios between loss of 18 m/z and 28 m/z were plotted as a function of the ratio of the M+1 protonated peak to the parent ion peak M.

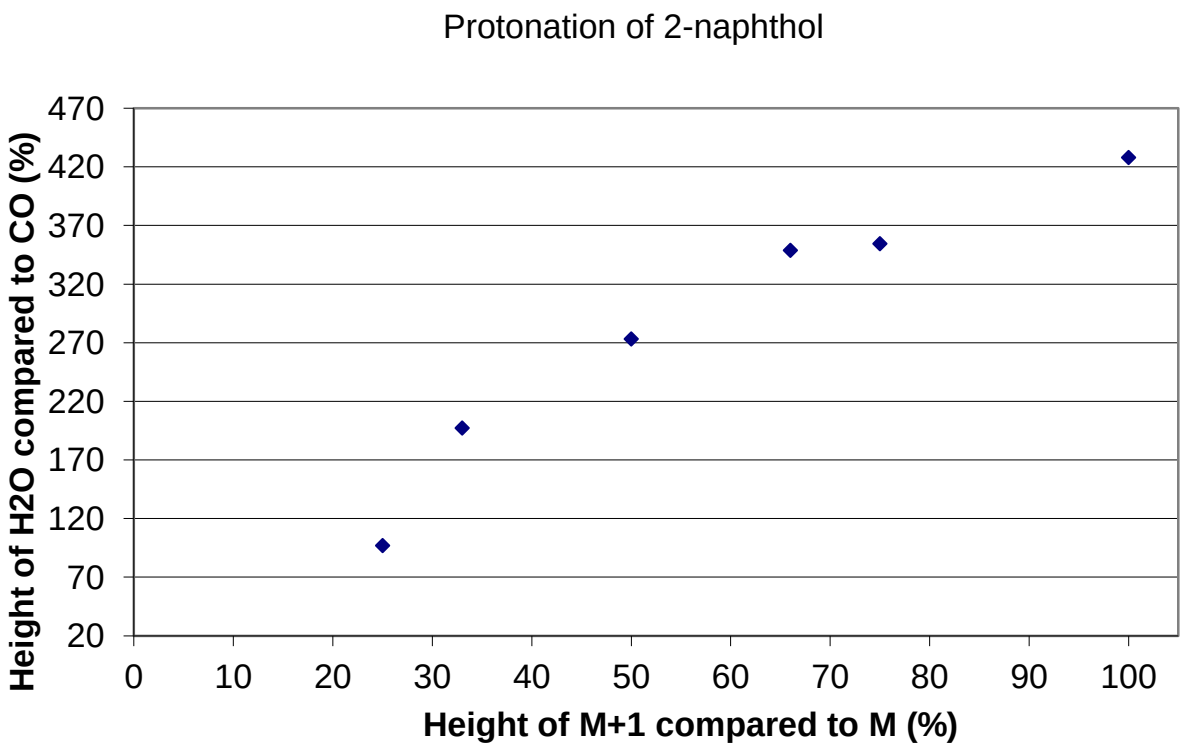

Figure 40: Graph showing the protonation of 2-naphthol using methane as a chemical ionization gas. The ratios between loss of 18 m/z and 28 m/z were plotted as a function of the ratio of the M+1 protonated peak to the parent ion peak M.

Based on these experiments, the proposed mechanism for the loss of water is shown below:

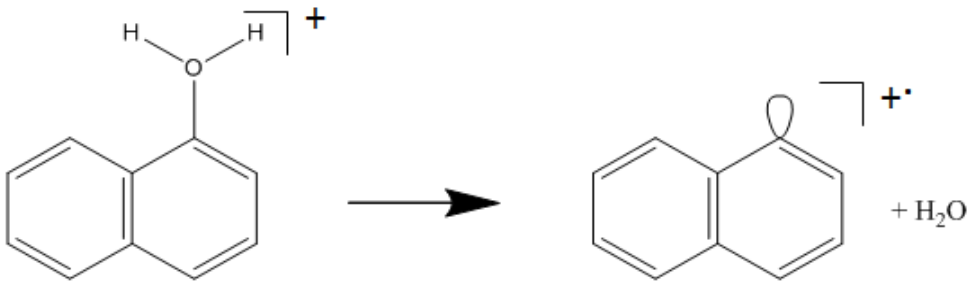

Figure 41: Proposed mechanism for the loss of water from protonated 1-naphthol

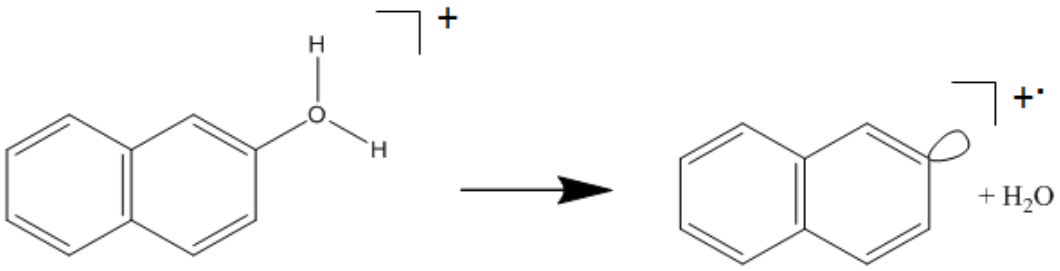

Figure 42: Proposed mechanism for the loss of water from protonated 2-naphthol

4.3 Protonation of the amines

Protonation was not possible for amino-substituted molecules nor bigger hydroxy-substituted PAHs since the ratio between the pressure of methane and the number of ions was not

optimal for protonation. Thus, breakdown diagrams of protonated 2-naphthylamine and protonated 2-aminoanthracene were obtained on a QTOF2 mass spectrometer using an ESI source.

For the protonated 2-naphthylamine, which is the smallest amino-substituted PAH studied, the dominant loss was NH_3 loss and goes as high as 65% intensity around a center-of-mass collision energy of 6 eV. Proton loss is also seen as the second-most dominant channel but doesn't go as high as NH_3 loss. The intensity of proton loss peaks around 15% at center-of-mass collision energy of 5 eV. HCN loss is the third-most dominant channel for protonated 2-naphthylamine, peaking around 10% intensity at around center-of-mass collision energy of 4.5 eV. The proposed mechanism for the loss of ammonia for 2-naphthylamine is as follow:

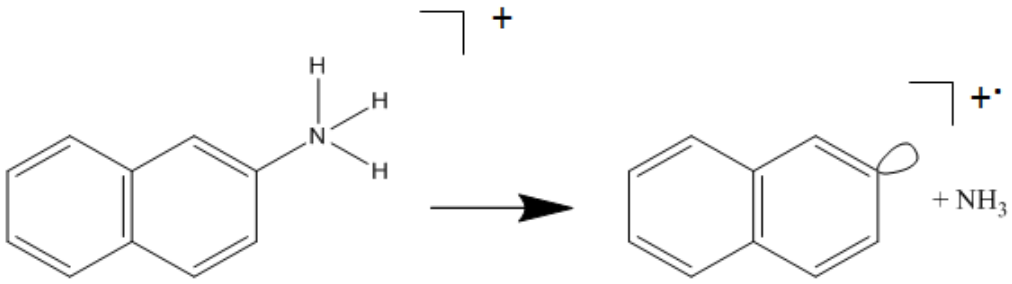

Figure 43: Proposed mechanism for the loss of ammonia from protonated 2-naphthylamine

The bond dissociation energy for N-H on a NH_3 group is around 435 kJ/mol while the bond dissociation energy for C-H on an aromatic ring is around 431 kJ/mol.[20] Since the two bond dissociation energies are so close, the proton could come from the NH_3 group and from the PAH

ring, given they have enough energy to dissociate. The proposed mechanism for proton loss is as follow:

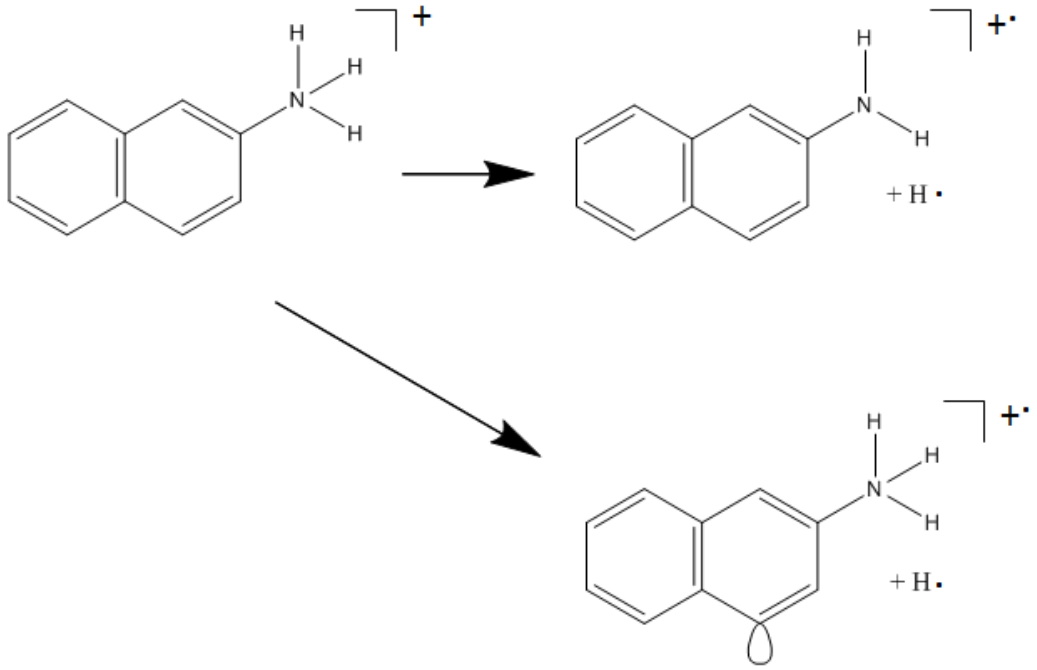

Figure 44: Proposed mechanism for the loss of hydrogen from protonated 2-naphthylamine. The first possibility is proton loss from the NH_3 group (top) and the second possibility is hydrogen loss for the aromatic ring (bottom).

As for protonated 2-aminoanthracene, the same experiment as for 2-naphthylamine was repeated to study if the same pattern was repeating for a larger protonated PAH. For this protonated PAH with three rings, the dominant loss now is hydrogen loss and not ammonia loss. The second-most dominant loss is NH_3 loss for protonated 2-aminoanthracene. This is compared in the following figures:

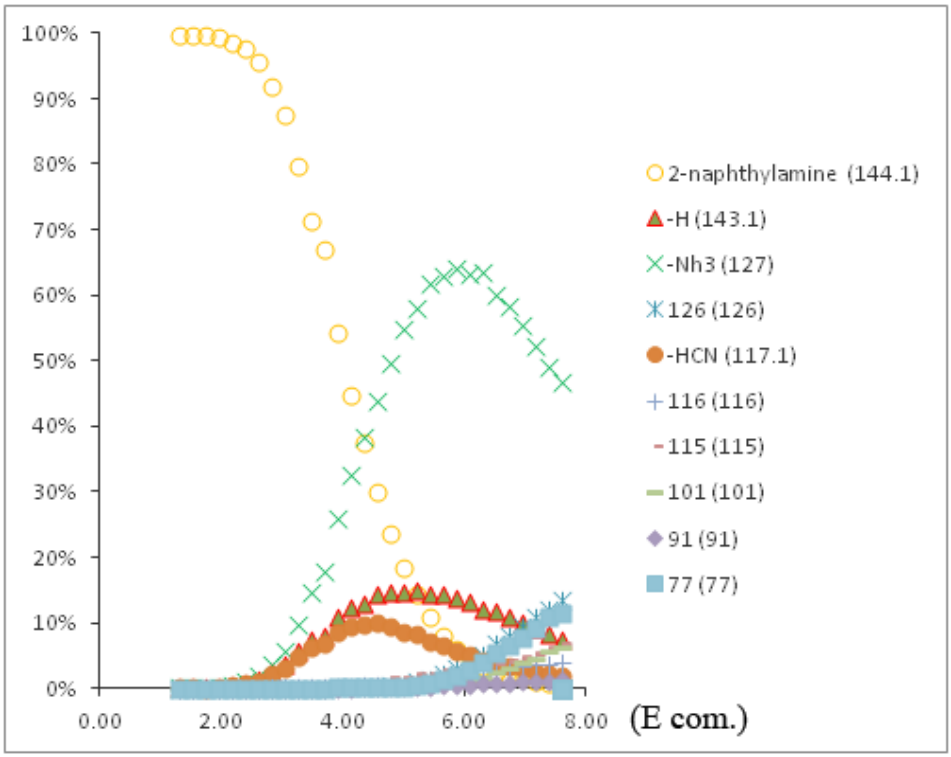

Figure 45: Breakdown diagram of protonated 2-naphthylamine using MS/MS on a Q-TOF instrument. The collision energy used was from 6.00 to 35.00 eV (E lab.) by increments of 1. The breakdown diagram was plotted using the relative intensities of each fragment ion.

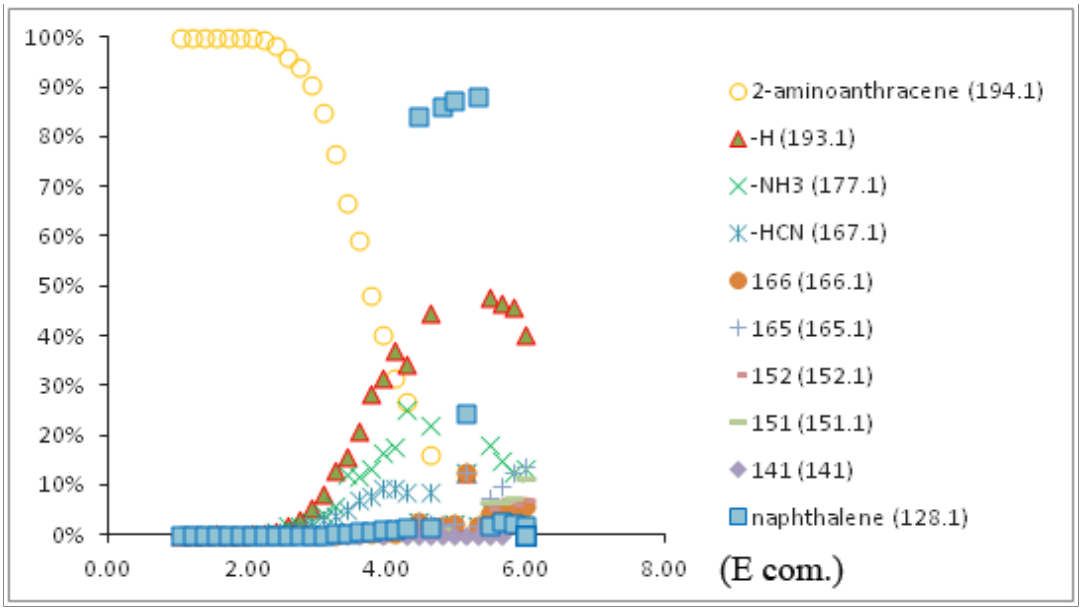

Figure 46: Breakdown diagram of protonated 2-aminoanthracene using MS/MS on a Q-TOF instrument. The collision energy used was from 6.00 to 35.00 eV (E lab.) by increments of 1. The breakdown diagram was plotted using the relative intensities of each fragment ion.

As seen in these previous figures, ammonia loss is not the most dominant loss anymore for a protonated PAH bigger than two rings. The most dominant loss is now hydrogen loss. To compare, for 2-naphthylamine, ammonia loss has a relative intensity of about 65% whereas for 2-aminoanthracene, ammonia loss has a relative intensity of about 20%. The relative intensity of ammonia loss dropped significantly. As for hydrogen loss, for 2-naphthylamine, the relative intensity is about 15% whereas it is about 50% for 2-aminoanthracene. The intensity of hydrogen loss is significantly higher when a ring is added to the protonated PAH. Again, the bond dissociation energy for a hydrogen on an aromatic ring versus on a NH_3 group differ for approximately 4 kJ/mol.[20] This means that the hydrogen could come either from the NH_3 group

or the aromatic or both. A proposed mechanism for ammonia loss and hydrogen loss from protonated 2-aminoanthracene is shown below:

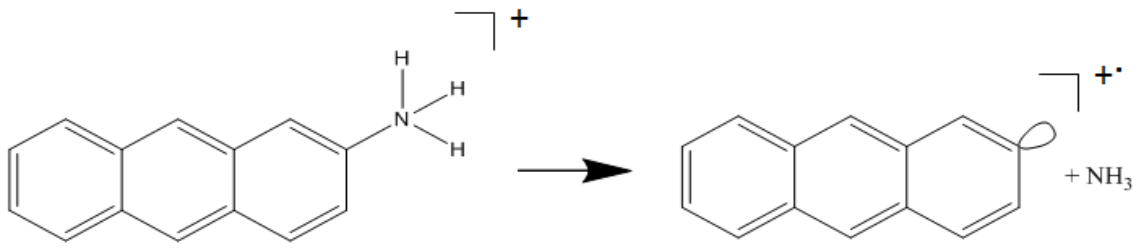

Figure 47: Proposed mechanism for the loss of ammonia from protonated 2-aminoanthracene

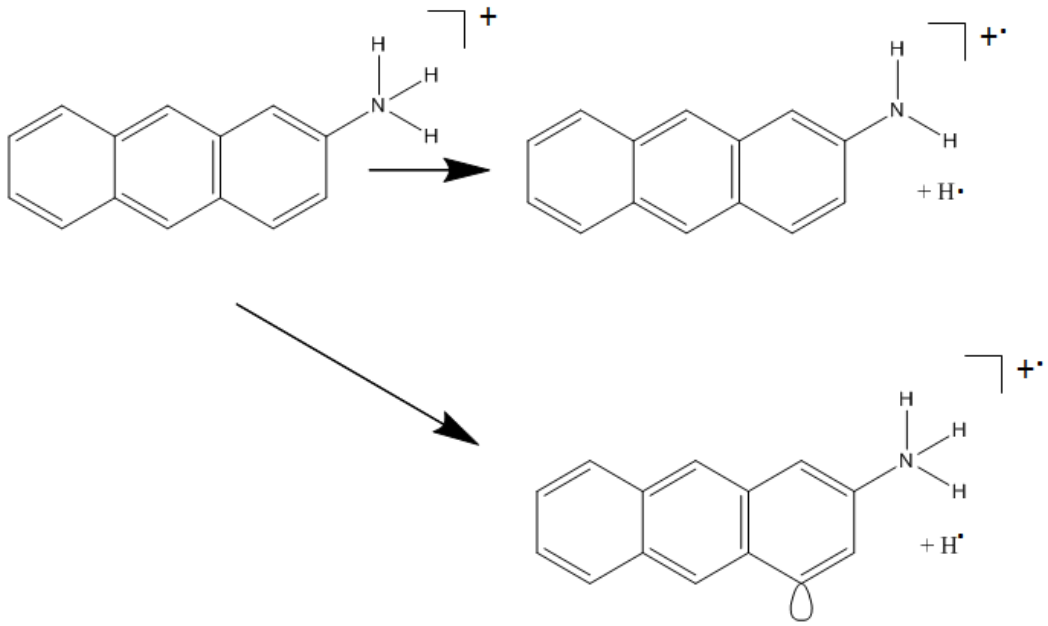

Figure 48: Proposed mechanism for the loss of a hydrogen from protonated 2-aminoanthracene. The first possibility is hydrogen loss from the NH_3 group (top) and the second possibility is hydrogen loss for the aromatic ring (bottom).

By extrapolating to the bigger PAHs than three rings, hydrogen loss would probably be the most dominant loss and ammonia would become non-existent or very small. Since that in the interstellar medium, PAHs of at least 50 carbons are believed to exist, hydrogen loss from protonated amino-substituted PAHs would be the dominant loss and the most important loss to take into account to extrapolate to larger systems. Based on the bond dissociation energy of proton loss from a NH_3 group and an aromatic ring, hydrogen loss would occur most probably on both sites. Thus, protonated amino PAHs are unlikely to produce NH_3 in the ISM, drawing into question the catalytic role of PAHs in this process.

Chapter 5. Conclusions

The gas-phase ion chemistry of hydroxy-substituted and amino-substituted polycyclic aromatic hydrocarbons and their protonated counterparts were studied using a VG-ZAB sector mass spectrometer and a QTOF2 mass spectrometer. Hydroxy-substituted PAHs were found to lose carbon monoxide whereas amino-substituted PAHs were found to lose HCN. The remaining fragments from carbon monoxide and HCN loss were found to be closed rings. For ionized 1-naphthol, 2-naphthol, 1-naphthylamine and 2-naphthylamine, the remaining fragment was found to be ionized indene. For ionized 9-phenanthrol, the remaining fragment was found to be ionized fluorene. All other fragments were found using DFT calculations with the B3LYP functional. These trends can be extrapolated to the more meaningful and bigger PAHs of more than 50 carbons.

Protonation was achieved for 1-naphthol and 2-naphthol using a high-pressure source and methane. It was found that carbon monoxide loss came exclusively from the carbon-13 contribution of the parent ion and that H_2O loss was from the protonated 1-naphthol and 2-naphthol. For the protonation of amino-substituted PAHs, the most dominant channel using a QTOF2 breakdown diagram was NH_3 loss for 2-naphthylamine and hydrogen loss from 2-aminoanthracene, ammonia loss being the second-most dominant loss. Extrapolating to the bigger PAHs of 50 carbons or more, the most dominant loss would most probably be hydrogen loss from either the aromatic ring or the NH_3 group based on their bond dissociation energies, which are very close.

The goal of this project was to extrapolate our findings to the bigger PAHs of more than 50 carbons believed to populate the interstellar medium. Hydroxy-substituted PAHs lose spontaneously carbon monoxide and amino-substituted PAHs lose HCN. The remaining structure is always a closed-ring structure as explained previously. As for protonated hydroxy-substituted PAHs, water was spontaneously lost and carbon monoxide loss was only from the carbon-13 contribution of the M+1 peak. However, for amino-substituted PAHs that were studied using a QTOF2, as the PAHs got bigger, the dominant channel was hydrogen loss, but for the smallest ones like 2-naphthylamine, the dominant channel was found to be ammonia loss. In the future, it would be interesting to explore the reactions between clusters of PAHs and to study the insertion of water and ammonia in PAHs that have lost a hydrogen to compare them to the protonated hydroxy-substituted PAHs and amino-substituted PAHs. Again, extrapolation to bigger PAHs will be important to compare the smaller systems studied to the systems believed to be found in the interstellar medium.

Contributions to Original Research

1- An EI source using a VG-ZAB mass spectrometer was used to determine a trend for the fragmentation patterns using MIKES, CID and MI/CID of hydroxy-substituted PAHs and amino-substituted PAHs and how they related to one another. Ten different PAHs were studied: 1-naphthol, 2-naphthol, 1-phenanthrol, 9-phenanthrol, 1-hydroxypyrene, 1-naphthylamine, 2-naphthylamine, 1-aminoanthracene, 2-aminoanthracene, 1-aminopyrene.

2- The effects of protonating 1-naphthol and 2-naphthol on the VG-ZAB mass spectrometer using a high-pressure source with the help of methane was investigated for the first time.

3- Comparison with the protonation of 2-naphthylamine and 2-aminoanthracene on a QTOF2 apparatus was achieved for the first time. It would be therefore useful to try protonating these PAHs using different mass spectrometers and comparing the results.

References

[1] Joblin C.; Tielens A.G.G.M., *EAS Publications Series*, **2011**, *46*, 427-440

[2] Snow T. P.; Le Page V.; Keheyan Y.; Bierbaum V. M., *Nature*, **1998**, *391*, 269-260

[3] Sebree J. A.; Kislov V. V.; Mebelb A. M.; Zwier T. S., *Faraday Discuss*., **2010**, *147*, 231–249

[4] Sakon I.; Onaka T.; Ishihara D.; Ootsubo T.; Yamamura I.; Tanabe T.; Roellig T. L., *ApJ*, **2004**, *609*, 203-219

[5] Chan K.-W.; Roellig T. L.; Onaka T.; Mizutani M.; Okumura K.; Yamamura I.; Tanabe T.; Shibai H.; Nakagawa T.; Okuda H., *ApJ*, **2000**, *546*, 273-278

[6] Tielens A.G.G.M., *Annu. Rev. Astron. Astrophys*., **2008**, *46*, 289–337

[7] Sakon I.; Onaka T.; Ishihara D.; Ootsubo T.; Yamamura I.; Tanabe T.; Roellig T. L., *ApJ*, **2004**, *609*, 203-219

[8] Mayer P. M., The Encyclopedia of Chemical Physics and Physical Chemistry Volume II: Methods, 2001, 1147-1174

[9] NIST Chemistry Webbook, NIST standard reference database national institute of standards and technology, 2011-2014

[10] Sigma-Aldrich, Sigma-Aldrich Co. LLC., 2011-2013

[11] Gaussian 09, Revision D.01, Frisch, M. J.; Trucks, G. W.; Schlegel, H. B.; Scuseria, G. E.; Robb, M. A.; Cheeseman, J. R.; Scalmani, G.; Barone, V.; Mennucci, B.; Petersson, G. A.; Nakatsuji, H.; Caricato, M.; Li, X.; Hratchian, H. P.; Izmaylov, A. F.; Bloino, J.; Zheng, G.; Sonnenberg, J. L.; Hada, M.; Ehara, M.; Toyota, K.; Fukuda, R.; Hasegawa, J.; Ishida, M.; Nakajima, T.; Honda, Y.; Kitao, O.; Nakai, H.; Vreven, T.; Montgomery, J. A., Jr.; Peralta, J. E.; Ogliaro, F.; Bearpark, M.; Heyd, J. J.; Brothers, E.; Kudin, K. N.; Staroverov, V. N.; Kobayashi, R.; Normand, J.; Raghavachari, K.; Rendell, A.; Burant, J. C.; Iyengar, S. S.; Tomasi, J.; Cossi, M.; Rega, N.; Millam, N. J.; Klene, M.; Knox, J. E.; Cross, J. B.; Bakken, V.; Adamo, C.; Jaramillo, J.; Gomperts, R.; Stratmann, R. E.; Yazyev, O.; Austin, A. J.; Cammi, R.; Pomelli, C.; Ochterski, J. W.; Martin, R. L.; Morokuma, K.; Zakrzewski, V. G.; Voth, G. A.; Salvador, P.; Dannenberg, J. J.; Dapprich, S.; Daniels, A. D.; Farkas, Ö.; Foresman, J. B.; Ortiz, J. V.; Cioslowski, J.; Fox, D. J. Gaussian, Inc., Wallingford CT, 2009.

[12] High Performance Computing Virtual Laboratory, Compute Calcul Canada, 2011-2014

[13] Boyd D. R.; Daly J. W.; Jerina D. M., *Biochemistry*, **1972**, *11*, 1961-1966

[14] Zhu L.; Bozzelli J. W.; *J. Phys. Chem. A*, **2003**, *107*, 3696-3703

[15] Alata I.; Omidyan R.; Broquier M.; Dedonder C.; Dopferc O.; Jouvetab C.; *Phys. Chem. Chem. Phys*., **2010**, *12*, 14456–14458

[16] Auea D. H.; Guidonia M.; Betowski L.D.; *Int. J. Mass Spec*., **2000**, *201*, 283–295

[17] Joblin C.; Tielens A.G.G.M., *EAS Publications Series*, **2011**, *46*, 373-379

[18] Ricca A.; Bauschlicher C. W. Jr.; Allamandola L. J., *ApJ*, **2011**, *727*, 128-133

[19] Lossing F. P.; Holmes J. L., *J. Am. Chem. Soc.*, **1984**, *106* (23), 6917–6920

[20] Cottrell T. L., The Strengths of Chemical Bonds, 2d ed., Butterworth, London, **1958**; Darwent B. de B., National Standard Reference Data Series, National Bureau of Standards, *31*, Washington, **1970**; Benson S. W., *J. Chem. Educ*. 42:502, **1965**; Kerr J. A., Chem. Rev. 66:465, **1966**